

# Transport of variable-density solute plumes in beach aquifers in response to oceanic forcing

R. Bakhtyar <sup>\*a,b,c</sup>, A. Brovelli <sup>c</sup>, D.A. Barry <sup>c</sup>, C. Robinson <sup>d</sup>, L. Li <sup>e</sup>

<sup>a</sup> Present address: Department of Environmental Sciences and Engineering, The University of North Carolina, Chapel Hill, NC 27599-7431, USA. Email: [roham.bakhtyar@unc.edu](mailto:roham.bakhtyar@unc.edu)

<sup>b</sup> Present address: Coastal and Hydraulics Laboratory, US Army Engineer Research and Development Center, Vicksburg, MS 39180-6133, USA

<sup>c</sup> Laboratoire de technologie écologique, Institut d'ingénierie de l'environnement, Faculté de l'environnement naturel, architectural et construit (ENAC), Station 2, Ecole polytechnique fédérale de Lausanne (EPFL), 1015 Lausanne, Switzerland. Emails: [alessandro.brovelli@epfl.ch](mailto:alessandro.brovelli@epfl.ch), [andrew.barry@epfl.ch](mailto:andrew.barry@epfl.ch)

<sup>d</sup> Department of Civil and Environmental Engineering, University of Western Ontario, London, Ontario N6A 5B9, Canada. Email: [crobinson@eng.uwo.ca](mailto:crobinson@eng.uwo.ca)

<sup>e</sup> School of Civil Engineering, University of Queensland, St. Lucia, Queensland 4072, Australia. Email: [l.li@uq.edu.au](mailto:l.li@uq.edu.au)

Published: *Advances in Water Resources*, 2013

---

\* Author to whom all correspondence should be addressed. Ph. +1 (919) 525-6217, Fax. +1 (919) 966-7115

**ABSTRACT:** A comprehensive numerical study was undertaken to investigate transport of a variable-density, conservative solute plume in an unconfined coastal aquifer subject to high and low frequency oceanic forcing. The model combined variable-density saturated flow for groundwater and solute transport, and wave hydrodynamics from a 2D Navier-Stokes solver. A sinusoidal tidal signal was specified by implementing time-varying heads at the seaward boundary. The solute plume behavior was investigated under different oceanic forcing conditions: no forcing, waves, tide, and combined waves and tide. For each forcing condition, four different injected solute densities (freshwater, brackish water, seawater, brine) were used to investigate the effects of density on the transport of the injected plume beneath and across the beach face. The plume's low-order spatial moments were computed, viz., mass, centroid, variance and aspect ratio. The results confirmed that both tide- and wave-forcing produce an upper saline plume beneath the beach face in addition to the classical saltwater wedge. For the no-forcing and tide-only cases (during rising tides), an additional small circulation cell below the beach face was observed. Oceanic forcing affects strongly the solute plume's flow path, residence time and discharge rate across the beach face, as well as its spreading. For the same oceanic forcing, solute plumes with different densities follow different trajectories from the source to the discharge location (beach face). The residence time and plume spreading increased with plume density. It was concluded that simulations that neglect the effect of waves or tides cannot reproduce accurately solute plume dispersion and also, in the case of coasts with small waves or tides, the solute residence time in the aquifer.

*Keywords:* Contaminant transport; Conservative tracer; Density-driven circulation; Hydrodynamics; High and low frequency motions; Coastal aquifer; Variable-density groundwater

## Abbreviations

HT	High Tide
LT	Low Tide
NS	Navier-Stokes
RANS	Reynolds-Averaged Navier-Stokes
SWL	Still Water Level
TKE	Turbulent Kinetic Energy
VOF	Volume-Of-Fluid

## Symbols

<i>Variable</i>	<i>Description</i>	<i>Dimensions</i>
$A$	tidal amplitude	L
$C$	concentration	$M L^{-3}$
$h_{tide}$	time-varying tidal head	L
$h_f$	equivalent freshwater head	L
$H$	water wave height	L
$K_f$	hydraulic conductivity	$L T^{-1}$
$k$	turbulent kinetic energy	$L^2 T^{-2}$

$L$	model domain length	L
$m$	normalized solute mass in the aquifer	-
$M_0$	zero-order moment	M
$M_1$	first-order spatial moment	L
$M_{11}$	covariance	$L^2$
$M_2$	second-order spatial moment	$L^2$
$t$	time	T
$T$	wave period	T
$x, z$	horizontal and vertical directions, respectively	L
<i>Greek</i>		
$\varepsilon$	turbulence dissipation rate	$L^2 T^{-3}$
$\sigma$	covariance tensor	$L^2$
$\rho$	fluid density	$M L^{-3}$
$\rho_p$	solute plume density at the point of injection	$M L^{-3}$
$\omega$	tidal angular frequency	$T^{-1}$

## 1. Introduction

Groundwater quality in nearshore aquifers is affected by seawater intrusion (e.g., [1,2]), as well as localized contamination due, for example, to accidental pollutant discharges from urban areas, industrial plants and landfills located near the shoreline (e.g., [3-5]). Nearshore groundwater processes, including tides, waves and changes in groundwater conditions arising from pumping and climatic stresses, play an important role in the exchange of solutes across the aquifer-ocean interface [6-8].

The influence of tidal effects on saltwater intrusion and nearshore aquifer dynamics has been studied thoroughly (e.g., [6,9-15]). Four approaches have been used to investigate groundwater flow and transport processes driven by tidal forcing: (i) field experiments [9]; (ii) laboratory measurements [6,15]; (iii) analytical models [16]; and (iv) numerical simulations [12,13,17,18]. Tides control the salinity distribution in the nearshore aquifer, affect the shape and position of the intruding saltwater wedge, as well as modify groundwater flow patterns (e.g., [4,13,19-24]). Robinson et al. [11] explored salt-freshwater mixing in a nearshore aquifer subject to tidal forcing and found that the tide-induced flows and saltwater transport leads to the formation of an upper saline plume over discharging fresh groundwater. This was shown to enhance salt-freshwater mixing.

Studies have examined the extent to which tide-induced circulation affects also solute fate in nearshore aquifers. Two scenarios can be distinguished. In the first, solutes are released in the open water (i.e., offshore) and reach the beach face through oceanic currents and waves, such as in the case of accidental oil spills (e.g., [25-27]). The second scenario considers the case of land-derived solutes released onshore, near the coastline. In particular, Zhang et al. [28,29], Boufadel et al. [6,30] and Brovelli et al. [17], through laboratory tank experiments and numerical modeling, examined the effects of tides on variable-density solute plumes. They observed that the solute mostly discharged across the beach face, but that tides influence the shape and spreading of the plume. Increased solute spreading

due to oceanic fluctuations was also confirmed by Elfeki et al. [31]. Robinson et al. [12] showed that tidal circulation increases dissolved oxygen availability in the sediments and therefore may promote oxidation of pollutants prior to discharge. It can be concluded that (i) tidal forcing modifies the rate of discharge of conservative solutes; (ii) the salinity distribution near the shoreline is controlled by the tidal amplitude and regional hydraulic gradient, and (iii) tide-induced groundwater circulation near the beach face leads to the formation of an upper saline plume in addition to the lower saltwater wedge.

In addition to the influence of tides on nearshore groundwater dynamics, wave effects need to be accounted for [32]. The exchange of fluid across the beach face during each wave period influences circulation patterns and the salinity distribution, which could affect solute transport in the aquifer [10,33]. Wave run-up increases saltwater infiltration through the beach face, which creates a mixing zone (upper saline plume) beneath the beach face [4,7,22]. Recently, Xin et al. [8] examined the individual and combined effects of waves and tides on groundwater flow and saltwater transport in a nearshore aquifer. They combined SUTRA [34], a variably saturated groundwater flow model, with BeachWin [35], to simulate the effects of linear incoming waves. They observed that coupled tides and waves increase the circulation of pore-water (circulation of seawater or circulation of land-derived pore-water), enhancing the width and thickness of the upper saline plume. BeachWin is based on the depth-integrated shallow water flow equations and cannot simulate the complex flow, turbulence fields and vertical velocities that may affect wave-induced fluxes across the beach face [7].

The objective of this study is to analyze the effect of oceanic fluctuations (high- and low-frequency ocean forcing, i.e., waves and tides, respectively) on the fate of solutes released in a nearshore aquifer. Simulation results for simplified conditions (e.g., no fluctuations or tide-only) are compared with those obtained under more complex conditions where all forcing are considered. This enables identification of conditions for which the effect of oceanic fluctuations can be neglected. The

simulations are pertinent to polluted water that is released into the aquifer near the shoreline, such as in the case of septic tanks, industrial plants or landfills (e.g., [3,5,36]). Contaminated waters can be denser than ambient freshwater, which results in more complex transport pathways [17,29]. For this reason, the simulations presented here consider density differences between the ambient water and injected solute plume in addition to the density effects between the ambient groundwater and circulating saltwater. The model has not been validated against experimental data for the conditions considered in this manuscript since suitable data sets are not available. But, the predictive capabilities of the each sub-module have been tested previously (i.e., [12,17,37,38]) and good agreement was found considering different conditions. Thus, we believe that the model used in this study is to some extent validated.

## **2. Methodology**

Bakhtyar et al. [37-39] developed a 2D (cross-shore) numerical study to simulate water flow in the surf and swash zones as well as in the nearshore aquifer. Fluid motion in the ocean was simulated using the Navier-Stokes (NS) equations. Comparison of model predictions with experimental data on wave-induced water table fluctuations, sediment transport and beach profile changes indicated that the model is well suited to simulate the effect of incoming waves on in/exfiltration fluxes across the beach face. The main features of the numerical study are summarized in the following.

### *2.1. Variable-density groundwater flow and transport model*

SEAWAT Version 4 [40] was used to simulate variable-density groundwater flow and solute transport in a nearshore aquifer subject to dynamic fluctuations at the seaward boundary. SEAWAT is a variable-density saturated flow model based on the equivalent freshwater head formulation that couples MODFLOW-2000 [41] for groundwater flow with MT3DMS v. 5.0 [42] for solute transport.

The groundwater flow and solute transport model was first run using a static sea level (Still Water Level, SWL) to obtain the steady-state groundwater heads and salt distribution. Following [17], the nearshore free-water zone (the sea) was approximated in SEAWAT using a fictitious medium with a high hydraulic conductivity ( $10^6 \text{ m d}^{-1}$ ). A constant head condition was set on the seaward and landward boundaries, while an impermeable no-flow boundary was assumed along the bottom boundary (Fig. 1).

## 2.2. Modeling of oceanic fluctuations

The effect of wave motion on the nearshore aquifer dynamics was simulated following [38,39]. The 2D RANS wave-motion model of [37,43] was used to simulate the seawater elevation above the beach face resulting from the oceanic waves. The model combines the continuity and momentum formulation of the incompressible NS equations with a  $k$ - $\epsilon$  turbulence closure and VOF technique. The generating-absorbing boundary condition was used at the offshore boundary to generate incoming waves while adsorbing reflected waves [43-45].

Coastal hydrodynamics were linked to the aquifer at the beach face. Head boundary conditions were applied at the beach face (in the free-water section of the domain) and directly above the watertable (in the aquifer). The head at the boundary, which accounted for both waves and tides, was computed with:

$$h_{tot}(t) = h_{wave}(t) + A \cos(\omega t), \quad (1)$$

where  $h_{tot}$  is total head (sum of wave and tide heights),  $h_{wave}$  is the elevation of the sea surface computed using the NS solver,  $t$  is time,  $A$  is the tidal amplitude and  $\omega$  is the tidal angular frequency. In the simulations with the tide only,  $h_{wave}$  was replaced by the SWL. For the case of combined waves and tides, the wave signal was computed assuming a constant SWL in the NS solver.



For the simulations with oceanic forcing, the steady-state head and salt distributions were used as initial conditions and a time-variable head boundary (CHD-MODFLOW package) was applied at the seaward boundary. The entire simulation length was subdivided into multiple stress-periods. For each period, the initial and final sea elevations were calculated using the wave- and tide-motion simulators. Stress periods were divided further into time steps within SEAWAT using a constant head for each time step, computed as a linear interpolation between the initial and final head of the current stress period.

MODFLOW (and consequently SEAWAT) does not consider flow in the unsaturated zone. In this model, cells are de-activated if they are not fully saturated and if their bottom is below the watertable elevation. Due to the use of dynamic boundary conditions (tides and waves), the watertable elevation changes with time, therefore cells are deactivated while the watertable elevation is decreasing (e.g., during falling tides and wave backrush) and are re-activated as the watertable rises again (rising tide and wave runup). In MODFLOW, the re-wetting package was used to check at each time step which dry cells should become active. This introduces some non-linearities in the flow equations and significantly increases the computation time. A different but related problem rises with boundary conditions. Obviously, head boundary conditions can only be applied to a cell that is active at the beginning of a stress period. During the rising tide, at a specific location the head at the beginning of step  $i$  is higher than the head at the previous stress period ( $i - 1$ ). Therefore, at the beginning of period  $i$  the cell to which the boundary should be applied is inactive, because during the previous stress period the watertable elevation was lower than the elevation of the cell's bottom. In this case, the boundary condition is applied to a lower cell, permitting the re-wetting package to reactivate cells as they become saturated. This introduces some localized temporary artifacts in the flow field (i.e., cells that are in the saturated zone become sources of water).

### 2.3. Model setup

Numerical experiments similar to those of [39] were conducted, the major difference being that the groundwater flow model was extended landward to simulate the solute and salt transport in the aquifer and to decrease the influence of the landward boundary condition. A schematic of the model set-up and properties is provided in Fig. 1. Below, we refer to the injected contaminant as the solute plume.

Simulations were conducted for four different oceanic forcing conditions: (i) no oceanic forcing (i.e., density and hydraulic gradient-driven flow only), (ii) tide, (iii) waves, and (iv) combined waves and tide. We considered four different densities of the injected solute plume: (i) same as the ambient groundwater (freshwater), (ii) between freshwater and seawater (brackish), (iii) same as seawater (saltwater) and (iv) higher than seawater (brine). A small-scale field setup was used in this study. Therefore, the typical wave heights (~50 cm) and wave periods (between 5 and 10 s), and micro-tides amplitude (1 m) were set to simulate the wave motions for such experiments. Table 1 summarizes the properties of the 16 cases considered.

The numerical computations were stopped if there was no improvement in the head and salt-water wedge for two consecutive time steps. The computed steady-state groundwater flow and salt distributions in the coastal aquifer were used as initial conditions for the subsequent simulations. Then, the solute was injected and simulations were run until the solute was discharged from the aquifer (a residual tracer mass  $< 0.5\%$  of the injected mass was the threshold for ending the simulation).

Simulations with waves only were conducted using a phase-resolving approach (i.e., the full wave cycle was simulated spatially and temporally). For the groundwater flow, each 7-s wave period was divided in 14 equal stress periods (refers to periods over which the aquifer's boundary conditions are constant) to capture the head changes above the beach face and seawater infiltration/exfiltration. The

phase-resolving approach is more accurate but computationally demanding. Numerical experiments showed that the combination of waves and tides could not be simulated using the same methodology due to (i) the excessive computational demand and (ii) the changing watertable position due to the oceanic forcing (tides, in particular). With respect to the watertable position, within SEAWAT a fixed head condition must be applied above the watertable (and not on the beach face). The location of the watertable is however not known a priori and does not necessarily follow a predictable pattern, and so the phase-resolving approach could not be applied. The phase-averaged approach (results are an average of a wave) of [8] was therefore used. This approach is also much less computationally demanding. Xin et al. [8] compared the pseudo-steady state salt distribution and aquifer circulation obtained using the phase-resolving and phase-averaged approaches. They found similar results for the two cases and concluded that the main effect of waves on the circulation in the nearshore aquifer is due to wave setup, a feature that is retained by the phase-averaged simulations. Physically, their finding is expected since the groundwater flow driven by a rapidly fluctuating periodic boundary condition (i.e., waves) is small and constrained to locations very close to the beach face. The cumulative aquifer response occurs over longer periods and these are well characterized by the phase-averaged approach. This observation corresponds to using wave setup to simulate local flow beneath a beach face [46].

#### *2.4. Metrics for solute migration*

To compare the behavior of the solute plume between the different cases, the solute plume was characterized by computing the time-evolution of its spatial moments and covariance tensor (e.g., [47]). The total plume variance was computed as the trace of the covariance tensor, which is independent of the coordinate orientation. The total variance is an indication of aquifer water-solute mixing and spreading. The solute discharge rate across the beach face was estimated from the time derivative of the zero-order moment, and the aspect ratio of the plume was defined as the ratio of the second central

moments (computed along the plume's principal axes). Expressions for calculation of these moments are given in the Appendix. The total mass and discharge rate were normalized by the maximum mass in the aquifer to facilitate comparison of the different cases.

### 3. Results

In §3.1, the simulated solute plume with different densities and groundwater flow and transport dynamics in the absence of oceanic forcing are presented (Cases 1-4, Table 1). Groundwater flow patterns, and the simulated solute plumes (with different densities) under tidal forcing (Cases 5-8, Table 1), wave forcing (Cases 9-12, Table 1), and combined wave and tide forcing (Cases 13-16, Table 1) are presented in §3.2, 3.3 and 3.4, respectively.

#### 3.1 No oceanic forcing

Figure 2 shows that, in absence of tides and waves, the classical saltwater wedge forms with the density difference between ambient groundwater and seawater driving the recirculation of seawater through the aquifer. Streamlines can be divided into two parts: seawater recirculation through the saltwater wedge and discharge of ambient groundwater.

The  $0.25C_0$  (where  $C_0$  is the initial tracer concentration) contour shows the location of the (dense) solute plume (case 4) in the aquifer. Initially (panel a), the plume deflects the shallow flow streamlines, and the ambient groundwater discharges mostly above or near the SWL on the beach face. Deeper streamlines are not noticeably affected by the plume and their discharge occurs near the fresh/saltwater interface.

Within the seawater wedge, density-driven flow triggers a small circulation cell below the beach face (at a distance of about 25 m). As the tracer plume approaches the fresh/saltwater interface (panel b), the wedge steepens and the circulation cell below the beach face develops further. The presence of

the dense plume modifies the freshwater streamlines and as a result the location where land-derived solutes are discharged. When the plume contacts the seawater wedge, it merges and becomes part of it (panels c and d). At this stage, the plume and seawater wedge form a single body of water with density higher than ambient freshwater, which modifies the circulation near the aquifer/seawater wedge interface. This can be deduced from the shape of the streamlines in this region: normally they follow closely the sea/freshwater interface (panels a and b), but when the plume ‘touches’ the seawater wedge (panels c and d), streamlines bend and cross the seawater interface, following the plume/freshwater (compare panels b and d). Compared with the case without the dense solute plume (i.e., freshwater), the circulation patterns are profoundly modified (results not shown).

The circulation cell below the beach face eventually occupies more than half the thickness of the aquifer (panel c, ~27 m), and streamlines in the tracer plume are much steeper. The plume and seawater interface (dispersion zone) partially overlap. Streamlines in the freshwater aquifer (landward) are no longer affected by the dense plume. As the plume touches the beach face, the solute is progressively discharged and the tracer mass in the aquifer decreases.

The migration of the solute plume (different densities, Table 1) in the nearshore aquifer without oceanic forcing is illustrated in Fig. 3. Results are reported after 10, 20 and 30 d. The plume migration is controlled by the regional groundwater hydraulic gradient and the density contrast between the ambient freshwater and the solute plume [11]. Each plot in Fig. 3 also shows the location of the salt-freshwater interface, as given 0.5 normalized seawater salt concentrations. As the density of the solute plume increases, the plumes show greater vertical spreading and also alter the position and shape of the saltwater wedge (cf. Fig. 2). The higher density plumes cause steepening and a seaward migration of the salt-freshwater interface with the interface steepness increasing with solute plume density. Below,

subsequent simulations with oceanic fluctuations are compared with these results to identify the effects of waves and tides.

The plume's spatial moments in the coastal aquifer for cases 1-4 are shown in Fig. 4. Results are shown for the time variation of the zeroth moment (total mass), first spatial moment (centroid), aspect ratio (calculated along the plume's principal directions) and total plume variance. The time when 80% of the solute mass was removed (i.e.,  $t_{80}$ , referred to as the residence time) was also calculated. This time corresponds to the intersection between the zeroth spatial moment and the horizontal dashes in Fig. 4a. The moment analysis indicates that plume density influences its residence time and spreading characteristics (Table 2 and panels a, c and d of Fig. 4). In all cases, the plume variance does not vanish at long times because a small (less than 0.1%) amount of solute remained in the aquifer when the simulations were halted.

When the density contrast is negligible or small (fresh and brackish water), the horizontal groundwater flow driven by the regional hydraulic head gradient controls the migration and rate of solute discharge across the beach face. As the density increases, the solute plume spreads vertically downward while it is advected horizontally towards the ocean. Observe that the finite aquifer depth limits the plume's downward trajectory (Fig. 2), and so the results in Fig. 4 are specific to the aquifer geometry.

The solute plume density has some noticeable effects. First, with increasing density the flow path as indicated by the centroid location becomes longer (Fig. 4b), increasing the residence time (Table 2 and Fig. 4a). Second, near the fresh-seawater interface (Fig. 3), the plume movement is affected by density-driven flow circulations that transport the solute vertically, in particular for the seawater and brine cases ( $x > 20$  m in Fig. 4b). With increasing solute density, the movement in the vicinity of the beach face is due to the upward flow near the fresh-saltwater interface (Figs. 2 and 4).

After the initial increase in the aspect ratio during injection, the two cases with lower density show a sharp decrease (Fig. 4c). This is because the freshwater plume (and, to a lesser extent, the brackish plume, Fig. 2a,b) transport is predominantly horizontal (Fig. 4b), and so the plume stretches in the direction of groundwater flow. The aspect ratio slowly increases again when the front of the plume reaches the beach face. For the seawater and brine cases, the aspect ratio remains approximately constant and decreases after 30 d (because this is when the plume is being transported upwards and discharging). For the denser cases, the plume migration is driven by both the regional hydraulic gradient and density, as reflected by the plume shapes in Fig. 2. The total plume variance (Fig. 4d) suggests that, for the three cases with density greater than ambient, the spreading in the aquifer is similar (as they have a similar peak value), although the greatest spreading is reached at slightly different times. The largest total variance is obtained for the freshwater case. Of course, the variance decreases as the plume is discharged across the beach face.

### *3.2 Tidal forcing*

The flow streamlines and saltwater distributions in the aquifer for case 8 and after 30 d are shown in Fig. 5b (case 8 is densest case: Brine). The streamlines show that the tide leads to a phase-averaged (over a tidal cycle) groundwater circulation below the beach face through the intertidal zone and inland, as is evident in Fig. 5b for  $25 < x < 30$  m. Water infiltrates or exfiltrates across the beach face as the hydraulic gradient changes direction through the tidal cycle. This shallow tidal circulation leads to the formation of an upper saline plume ( $10 < x < 20$  m) through the intertidal region. The asymmetric water exchange across the interface is separated into density-driven circulation ( $10 < x < 20$  m) and tidally driven circulation ( $25 < x < 27$  m). Comparison of the no oceanic forcing (Fig. 5a) and the tidal forcing (Fig. 5b) cases shows that tidal effects push the saltwater wedge seaward ( $20 < x < 25$  m for no oceanic

forcing, cf.  $25 < x < 27$  m for tidal forcing), while the mixing (dispersion) zone width increases, consistent with the findings of [11].

Figure 6 shows the simulated solute plume for cases 5-8, 10, 20 and 30 d after solute injection. Due to the tide-induced seawater circulations (Fig. 5b) in the shallow intertidal region (the region of the aquifer that is directly influenced by tidal fluctuations), tides alter the transport pathways for the solute plumes (Fig. 6) compared with the case of no oceanic forcing (Fig. 3). This is particularly the case for the less dense plumes that travel in the upper part of the aquifer. Compared with the cases with no oceanic forcing, the plumes are transported downwards and around the tide-induced seawater circulation cell and then discharge near the low tide mark (e.g., Figs. 3a and 6a), consistent with [11,17,28,29]. For the denser plumes their transport pathways are more similar between the no oceanic forcing and tidal cases, more so as the travel time increases. This is because the movement of the plumes becomes strongly influenced by the upward flow associated with the saltwater wedge (e.g., Figs. 3c and 6c). As expected, as the density of the solute increases, the plume is transported deeper into the aquifer with greater vertical and horizontal spreading evident (e.g., Fig. 6c,d).

The 0.5 normalized salt concentration contour lines (Fig. 6) show both the upper saline plume and the lower saltwater wedge. Similar to the cases with no oceanic forcing, the position of the saltwater wedge was affected by the solute plume: As the solute plume approached the wedge, the position of the interface moved seaward according to the density contrast. Regardless of the plume density, the position and size of the upper saline plume was not modified by the solute plume. This occurs because the upper saline plume is formed due to advective flow driven by tidal forcing across the sloping beach face whereas the saltwater wedge is formed due to density-driven seawater circulation. Therefore, the density contrast associated with the solute plume does not alter the upper saline plume compared with the saltwater wedge.



Figure 7 gives metrics used to characterize the solute plumes for the different cases with tidal forcing. As expected, and similar to the cases with no oceanic forcing, the plume centroid sinks deeper into the aquifer as the plume density increases (Fig. 7b). The position of the centroid is deeper than for the no-forcing cases (1-4), again due to the shallow, tide-induced seawater circulation cell.

The temporal evolution of solute mass (Fig. 7a) follows a similar pattern for the four density cases (fast solute discharge initially followed by a period of lower solute discharge across the interface). The discharge rates decrease and the residence time ( $t_{80}$ , Table 2) increases as the density of the plume increases. Comparison with the no forcing cases (cases 1-4, Fig. 4a) shows that tidal forcing mostly reduces the solute discharge flux from the aquifer to the sea. In all cases the aspect ratio (Fig. 7c) decreases when the solute injection ends (after 6 d), i.e., the plume is elongated along the principal flow direction. This is because the discharging freshwater is restricted to a narrow zone between the upper saline plume and the saltwater wedge, which limits the transverse spreading of the plume. It also limits the effect of the solute density contrast between cases 5-8 (that would lead to a more rounded shape with an aspect ratio closer to unity). For the high-density solute plumes (cases 7 and 8), the longitudinal rather than transverse stretching is increased due to the interaction of the plume with the bottom (impermeable) boundary.

The shape and residence time of the plume are affected by the aquifer geometry including the distance between the solute source and the bottom boundary. While the quantitative results presented are specific to the setup used, the tide-induced oscillating flow in the aquifer increases the total variance of the plumes by at least 50%; compare the maxima in Figs. 4d and 7d. Initially, the variance increases with the plume density but, later, when the solute mass remaining in the aquifer is low, the freshwater and brackish plumes have higher variance and thus are more spread. This indicates that when most of the solute mass has been discharged and residual concentrations are relatively low,

denser solutes form a more compact plume. Denser solute plumes sink deeper into the aquifer and are influenced less by tidally oscillating flows (which decrease with depth in the aquifer), resulting in less plume dispersion. In the case of a degradable solute, this effect could influence its degradation as it would undergo less mixing with the ambient groundwater and recirculating seawater prior to discharge.

### 3.3 Wave forcing

Phase-averaged normalized salt concentrations in a nearshore aquifer subject to high frequency sea motion for case 12 (densest case: Brine) after 30 d is shown in Fig. 5c. The simulations show that wave forcing induces local circulation cells under the beach face ( $15 < x < 22$  m) (Fig. 5c, cf. [38,39]), which can affect solute transport and submarine groundwater discharge because they modify the pore water velocity (magnitude and direction) near the fresh/saltwater interface. The resulting salinity structure is similar to the cases with tidal forcing, with a distinct upper saline plume in addition to the saltwater wedge. The upper saline plume is formed by the saltwater infiltrating the beach face due to wave set-up, uprush and backwash. These two saline zones are separated by the discharging fresh groundwater. These results are consistent with those of [8]. A comparison of salt concentrations for tidal (Fig. 5b) and wave forcing (Fig. 5c) shows that the width of upper plume in the tidal case is larger. The extent of the upper saline plume depends on the specific wave and tidal forcing parameters adopted (e.g.,  $A$ ,  $\omega$ ,  $H$ ,  $T$ ) and, of course, the infiltration/exfiltration across the beachface.

Solute transport in the nearshore aquifer subject to wave forcing (cases 9-12) is shown in Fig. 8. The solute distributions differ from those with tidal effects (Fig. 6). Figure 8 reveals that, similar to tides, the wave-induced groundwater circulation modifies the discharge pathway. With waves present, the solute plume first migrates seaward along the top of the aquifer, but as it approaches the wave-induced flow circulation cell it is transported downwards. In the case of waves, however, the effects on solute distribution in the nearshore aquifer are controlled mainly by the upper saline plume. Due to the

high frequency of waves (relative to tides), the flow oscillations are attenuated a short distance from the beach face [37,48]. Tides instead have lower frequency and their signal penetrates further into the saturated zone, and so have a different influence on the shape and travel time of the plume (e.g., [17]).

Similar to the no oceanic forcing and tidal cases, the results illustrate that dense solute plumes sink deeper into the aquifer, and that the saltwater wedge is pushed further seaward as the plume density increases. A comparison of Figs. 3, 5 and 8 shows that, in response to the solute plume, the seawater wedge moved more for the waves or with no oceanic forcing cases and less for the cases with tidal forcing. While the conditions of the oceanic forcing for these four cases (i.e., cases 9-12) were the same (i.e., wave forcing), the positions of saltwater wedge were not.

Figure 9 shows the total mass, centroid, aspect ratio and total variance of the solute plume in the nearshore aquifer subject to wave forcing and for different densities. The change in mass with time reported in Fig. 9a shows that the average residence time is approximately 49 d, compared with 32 and 37 d for the no forcing and tidal cases, respectively (Table 2 and Fig. 9a). As for the tidal cases, the plume centroids are affected by the density contrast and the shallow seawater circulation cell. That means the trajectories of the centroids for the wave cases are deeper than for the cases with no oceanic forcing. The aspect ratio plot (Fig. 9c) shows that the shapes of the solute plume with waves and tides have similar features, i.e., the plume is stretched longitudinally. For cases 9-12, the maximum total variances are similar, between 20 and 25 m<sup>2</sup> and generally larger than variances for the tidal cases. The largest spreading is obtained after 20-25 d, with a value that is larger than the corresponding result for the cases with no oceanic forcing.

### *3.4 Combined wave and tidal forcing*

Interactions between groundwater and combined oceanic forcing can affect the local hydrodynamics, water exchange across the beach face and groundwater flow and solute transport. In this section, we model plume movement in response to combined waves and tides using the phase-averaged wave approach.

Phase-averaged normalized salt concentrations in a nearshore aquifer subject to combined wave and tidal forcing for case 16 (densest case: Brine) and after 30 d are shown in Fig. 5d. The salinity structure is qualitatively similar to the cases where waves and tides were considered separately. A comparison of Figs. 5a-d shows that the largest upper saline plume occurs for the combined wave and tide case (Fig. 5d), followed by the tidal (Fig. 5b) and wave cases (Fig. 5c). Although the size of the plumes depends on the specific parameters used in the simulations (tidal amplitude and wave frequency), the larger extent of the upper saline plume for the wave and tide case indicates that the effect of the two forcing mechanisms is roughly additive.

The migration of the conservative solute plume in the beach aquifer for combined waves and tide is illustrated in Fig. 10, while the plume's spatial moments in the aquifer for cases 13-16 are shown in Fig. 11. Results (both the patterns observed and the magnitude) are similar to those obtained for the cases with tides only. However, the solute flow path is lengthened due to the added wave effects, which produces a slightly larger saline plume beneath the beachface (cf. Figs. 6 and 8). For the freshwater plume, the residence time is increased relative to the tide-only case, but is less than for the simulations with waves only (Table 2). The brackish plume residence time is unchanged compared to that for tide only. For the larger densities (seawater and brine), the residence time is controlled partially by the plume reaching the impermeable bottom boundary, and is less than for the simulations with tide-only or wave-only. The possible explanation for these different behaviors is that the larger upper saline plume

induces higher discharge rates for the denser cases (seawater and brine), whereas for the freshwater-density case, the upper saline plume also increases the length of the solute flow path.

The 0.5 normalized salt concentration contour line (Fig. 10) shows both the upper saline plume and the lower saltwater wedge. The mixing zone widens ( $10 < x < 23$  m) compared with that for the waves ( $15 < x < 22$  m) and tide ( $12 < x < 21$  m) considered separately (Fig. 8). In addition, due to the effects of tide, the interface is pushed seaward compared with the wave-only cases. Similar to the cases with waves and tidal forcing (Figs. 6 and 8), the position of the saltwater wedge is pushed seaward by the denser solute plumes whereas the upper saline plume is not modified to any extent. For all cases under oceanic forcing, the plume density affects the saltwater wedge location much more noticeably than the upper saline plume (Figs. 6, 8 and 10).

#### 4. Discussion

The simulations indicate that oceanic fluctuations increase the residence time and dispersion of land-derived solute plumes in the coastal aquifer. This can be inferred from Figs. 4, 7, 9 and 11, panels a (residence time) and d (plume spreading). In addition, Table 2 reports the normalized residual solute mass in the aquifer at different times. Results are consistent with previous findings regarding the influence of tides on solute transport and discharge from the aquifer to the sea (e.g., [17,29,31]). For conditions where waves are the only oceanic forcing, the solute residence time is much larger than for conditions with no forcing or tidal forcing only. For example, for the neutrally buoyant plume, residence times are about 24, 26 and 44 d in the no-forcing, tide-only and wave-only cases, respectively. With combined tides and waves, the residence time is similar to but slightly larger than for the case with tides only (29 d). It is difficult to identify the reason for these differences, and in particular for the large residence time observed for the wave-only case. A possible explanation is that tidal forcing induces more significant mixing of the recirculating seawater in the upper saline plume

and the ambient discharging groundwater compared with waves, mainly because the wave-induced oscillating flows are attenuated rapidly in the aquifer. In other words, the flow fluctuations induced by waves cause much less displacement of the solute than the tidal oscillations [8]. In addition, waves are non-symmetric around the SWL (tides both refill and drain the aquifer, while waves induce more infiltration than exfiltration).

Concerning solute spreading, the total variance for the tide- and wave-only cases was similar, and was about 50% larger than that for the no-forcing condition. More solute dispersion was observed for combined waves and tides. The largest variance for this case was about twice that observed for the no-forcing conditions. To examine further the effect of increased residence time, the solute discharge rates across the beach face were computed (Fig. 12). Results are reported starting after the end of the injection period, when some changes in solute mass can be observed (day 10 onwards). The general trend is the same for all cases. Initially, while the plume migrates seawards the mass remains constant (the discharge rate is zero). Once the solute plume reaches the beach face, the rate of discharge increases (the normalized rate of change of solute mass in the aquifer,  $dm/dt$ , becomes more negative). The shape of the discharge curve is bell-shaped and symmetric for the freshwater cases for all oceanic forcing scenarios. The discharge curve becomes more skewed as the density of the solute plume increases and it takes more time for the solute to leave the aquifer. This is due to the opposing effects of density – which tends to maintain the solute near the impermeable lower boundary – and groundwater flow, which moves the solute towards the beach face. The rate of discharge and residence time for plumes of different densities shows consistent behavior, with most of the mass of the fresher plumes being discharged earlier.

Oceanic forcing in combination with the density effects associated with land-derived solute plumes significantly impact the flow circulations in the aquifer. Figure 5 reports the salt concentration

distribution, streamlines (white lines) and outline of the tracer plume (indicated by the  $0.25C_0$  contour line) 30 d after the end of the injection for the four different forcing conditions (phase-averaged flow for the brine case is shown). In all situations, the tracer plume and seawater wedge form a single body of denser water, which bends the streamlines and modifies the local flow direction. For the static and tidal cases, a circulation cell is visible below the beach face. For the tides, however, the convective cell is present. For the wave and combined tide-and-wave cases, the flow patterns are more complicated. Several small circulation cells and convergence zones form due to the transient effect of waves. Results for the combined tides and waves, obtained using the phase-averaged approach for waves, indicate that the circulation cells observed in the presence of waves are persistent (although in reality they are formed and destroyed during each wave cycle), and that their effect on the flow field is not negligible.

Our results have implications for the assessment and modeling of land-derived solute plumes. As mentioned earlier, most research so far has considered only tidal effects. Our simulations indicate that, along coastlines where oceanic waves have amplitudes similar to that of tides, neglecting the high frequency component could still provide a reasonable estimate of the solute's residence time in the aquifer, whereas the spreading would be underestimated. Results indicate that wave fluctuations should be considered in particular at locations where waves are the dominant forcing factor, i.e., along coasts adjoining the Mediterranean, Baltic or Caribbean seas. At these locations, the tidal amplitude is often small, in the range 0-10 cm [49]. For this condition, neglect of wave effects could lead to overestimates the solute residence time and underestimates of plume spreading. In addition, the modeling results indicate that waves drive a strong shallow circulation cell near the beach face, which is superimposed on the similar tide-induced circulation [8]. This shallow circulation (due to tides only) was found to enhance the degradation of organic solutes through increased oxygen availability in the shallow aquifer [12] and also increase nutrient turnover rates, which promotes biogeochemical processes in the intertidal zone (e.g., [50]). Due to the greater circulation observed in the combined wave-tide

simulations, it is expected that waves will increase further the oxygen availability in the shallow beach sediments. For situations dominated by wave forcing, increased oxygen availability in parallel to the residence time increase could have a beneficial effect on the natural attenuation of, for example, biodegradable organic solutes prior to their discharge to the sea.

It should, nevertheless, be noted that while this study advances modeling of solute transport in the nearshore aquifer, the results could be affected by the simplifying assumptions required to reduce the computational burden. In particular, unconfined aquifers fill and drain in response to oceanic fluctuations, and seepage faces can form [8,27,51,52]. Vadose zone flow and the seepage face are, however, not modeled in SEAWAT [52]. This is especially true in the case of high-frequency fluctuations (waves), because the wave period is similar or smaller than the time required by a single finite-difference cell in MODFLOW to saturate and drain. Boufadel et al. [30], however, observed that neglecting seepage face formation has a limited effect on solute transport predictions in aquifers subjected to tides, and while neglecting unsaturated flow can affect predictions for fine-grained sandy beaches, predictions are less influenced for medium- to coarse-grained beaches. The simulations conducted in this study were for a medium-grained sandy nearshore aquifer and so unsaturated flow and seepage face formation are considered to have only minor effects on the results.

## **5. Conclusions**

The influence of wave and tidal forcing on solute transport in the nearshore aquifer was investigated via a comprehensive numerical investigation. Our investigation showed that:

- The results confirmed previous investigations that in nearshore aquifers subject to tidal or wave forcing, there is an upper saline plume below the beach face in addition to the classical saltwater wedge within the aquifer. Only the latter exists for non-oceanic forcing conditions;



- The upper saline plume is largest for the combined wave-and-tide case followed by the tidal and wave cases. The extent of the upper saline plume depends on the specific wave and tidal forcing parameters;
- A flow circulation cell below the beach and just seaward of the seawater wedge/freshwater divide was observed for the static and tidal cases. This is primarily driven by density differences. For the cases with waves and combined tides and waves, the flow field is complex with numerous small circulation cells beneath the beach face;
- Variable density solute plumes entering the coastal aquifer modify the groundwater flow field. When the plume is far from the salt-freshwater interface, the streamlines are distorted and exit the aquifer near or above the SWL. As the solute plume approaches the seawater wedge, they merge and modify local flow patterns until the solute plume is removed;
- The density contrast associated with the solute plume has less effect on the upper saline plume than the saltwater wedge location;
- The solute plume density has a significant effect on the specific transport pathway and spreading of a solute plume in the aquifer. Plume spreading increased with density;
- While the solute residence time increased with increasing solute plume density in the absence of oceanic forcing, tides modulate the solute density effects. Solute plume transport around the upper saline plume – which occurs for all tidal cases – reduces solute density effects and decreases the solute discharge rate;
- Oceanic fluctuations increase the residence time and dispersion of land-derived solute plumes within the aquifer. For cases where waves are the only oceanic forcing, the residence time increase is much larger than for tide-only cases;

- The shape of the solute plume discharge curve across the beach face is bell-shaped and symmetric when the plume density is the same as the freshwater density, and becomes more skewed as the solute plume density increases. This is because of longer (and slower) solute transport paths to the beach face as the denser plumes move deeper into the aquifer;
- Where oceanic waves have small amplitude compared to tides, solute transport is only weakly affected by waves, which can be neglected. Similarly, where waves are the dominant forcing, tidal effects can be neglected. However, in general, as the effects of tides and waves induce the formation of an upper saline plume beneath the beach face and are additive, both combined wave and tidal effects should be accounted for.
- Although the simulations considered conservative solutes only, the findings regarding the residence time and the extent of mixing between the ambient groundwater and solute plume are relevant to predictions of degradation rates (e.g., larger residence time corresponds to potentially greater degradation of the solute in the aquifer prior to discharge).

## Acknowledgement

Support of the Swiss National Foundation (SNF 200021-135322) is acknowledged.

## Appendix. Spatial moments and covariance tensor

The low-order moments are defined as follows:

$$M_0(t) = \iint C(x, z, t) dx dz, \quad (\text{A-1})$$

$$M_{1x}(t) = \frac{\iint C(x, z, t) x dx dz}{M_0}, \quad (\text{A-2})$$

$$M_{11}(t) = \frac{\iint C(x, z, t)(x - M_{1x})(z - M_{1z}) dx dz}{M_0}, \quad (\text{A-3})$$

$$M_{2\chi}(t) = \frac{\iint C(x, z, t)(\chi - M_{1\chi})^2 dx dz}{M_0}, \quad (\text{A-4})$$

$$\boldsymbol{\sigma}(t) = \begin{bmatrix} M_{2x} & M_{11} \\ M_{11} & M_{2z} \end{bmatrix}, \quad (\text{A-5})$$

where  $M_0$  is the zero-order moment,  $\chi = x$  or  $z$ ,  $M_{1\chi}$  are the first-order moments,  $M_{2\chi}$  are the second-order moments, and  $M_{11}$  and  $\boldsymbol{\sigma}$  are the covariance and covariance tensor, respectively. The principle axes of the plume are given by the eigenvectors of  $\boldsymbol{\sigma}$ , while the aspect ratio is given by the transverse/longitudinal ratio of its eigenvalues. The plume centroid is given by  $(M_{1x}, M_{1z})$ .

## References

- [1] St. Germain DJ, Cohen DK, Frederick JJ. A retrospective look at the water resource management policies in Nassau County, Long Island. *J Amer Water Resour Assoc* 2008;44:1337–46.
- [2] Werner AD, Bakker M, Post VE, Vandenbohede A, Lu C, Ataie-Ashtiani B, Simmons CT, Barry DA. Seawater intrusion processes, investigation and management: Recent advances and future challenges. *Adv Water Resour* 2012. In press, doi: 10.1016/j.advwatres.2012.03.004.
- [3] Cox ME, Hillier J, Foster L, Ellis R. Effects of a rapidly urbanising environment on groundwater, Brisbane, Queensland, Australia. *Hydrogeol J* 1996;4:30–47.
- [4] Li L, Barry DA, Jeng D-S, Prommer H. Tidal dynamics of groundwater flow and contaminant transport in coastal aquifers. In *Coastal Aquifer Management—Monitoring, Modeling, and Case Studies*, Edited by A.H.-D. Cheng and D. Ouazar, chap. 6, pp. 115–141, 2004, Lewis, Boca Raton, Florida, USA.
- [5] Grassi S, Cortecchi G, Squarci P. Groundwater resource degradation in coastal plains: The example of the Cecina area (Tuscany–Central Italy). *Appl Geochem* 2007;22:2273–89.

- [6] Boufadel MC, Siudan MT, Venosa AD. Tracer studies in laboratory beach simulating tidal influences. *ASCE J Env Eng* 2006;132:616–23.
- [7] Bakhtyar R, Barry DA, Li L, Jeng D-S, Yeganeh-Bakhtiary A. Modeling sediment transport in the swash zone: A review. *Ocean Eng* 2009a;36:767–83.
- [8] Xin P, Robinson C, Li L, Barry DA, Bakhtyar R. Effects of wave forcing on a subterranean estuary. *Water Resour Res* 2010;46:W12505, doi:10.1029/2010WR009632.
- [9] Robinson MA, Gallagher D, Reay W. Field observations of tidal and seasonal variations in groundwater discharge to tidal estuarine surface water. *Ground Water Monit Remed* 1998;18:83–92.
- [10] Robinson C, Gibbes B, Li L. Driving mechanisms for groundwater flow and salt transport in a subterranean estuary. *Geophys Res Lett* 2006;33:L03402, doi: 10.1029/2005GL025247.
- [11] Robinson C, Li L, Barry DA. Effect of tidal forcing on a subterranean estuary. *Adv Water Resour* 2007;30:851–65.
- [12] Robinson C, Brovelli A, Barry DA, Li L. Tidal influence on BTEX biodegradation in sandy coastal aquifers. *Adv Water Resour* 2009;32:16–28.
- [13] Boufadel MC. A mechanistic study of nonlinear solute transport in a groundwater-surface water system under steady state and transient hydraulic conditions. *Water Resour Res* 2000;36:2549–65.
- [14] Destouni G, Prieto C. On the possibility for generic modelling of submarine groundwater discharge. *Biogeochemistry* 2003;66:171–86.
- [15] Mango AJ, Schmeeckle MW, Furbish DJ. Tidally induced groundwater circulation in an unconfined coastal aquifer modeled with a Hele-Shaw cell. *Geology* 2004;32:233–6.
- [16] Kacimov A, Abdalla O. Water table response to a tidal agitation in a coastal aquifer: The Meyer-Polubarinova-Kochina theory revisited. *J Hydrol* 2010;392:96–104.
- [17] Brovelli A, Mao X, Barry DA. Numerical modeling of tidal influence on density-dependent contaminant transport. *Water Resour Res* 2007;43:W10426, doi:10.1029/2006WR005173.

- [18] Licata IL, Langevin CD, Dausman AM, Alberti L. Effect of tidal fluctuations on transient dispersion of simulated contaminant concentrations in coastal aquifers. *Hydrogeol J* 2011;19:1313–22.
- [19] Ataie-Ashtiani B, Volker RE, Lockington DA. Tidal effects on sea water intrusion in unconfined aquifers. *J Hydrol* 1999;216:17–31.
- [20] Mao X, Enot P, Barry DA, Li L, Binley A, Jeng D-S,. Tidal influence on behaviour of a coastal aquifer adjacent to a low-relief estuary. *J Hydrol* 2006;327:110–27.
- [21] Kuan WK, Jin G, Xin P, Robinson C, Gibbes B, Li L. Tidal influence on seawater intrusion in unconfined coastal aquifers. *Water Resour Res* 2012;48:W02502, doi:10.1029/2011WR010678.
- [22] Guo Q, Li H, Boufadel MC, Sharifi Y. Hydrodynamics in a gravel beach and its impact on the Exxon Valdez oil spill. *J Geophys Res Oceans* 2010;115:C12077, doi: 10.1029/2010JC006169.
- [23] Mao X, Prommer H, Barry DA, Langevin CD, Panteleit B, Li L. Three-dimensional model for multi-component reactive transport with variable density groundwater flow. *Env Model Softw* 2006b;21:615–28.
- [24] Werner AD, Lockington D A. Tidal impacts on riparian salinities near estuaries, *J Hydrol* 2006;328:511–22.
- [25] Guo Q, Li H, Boufadel MC, Sharifi Y. Hydrodynamics in a gravel beach and its impact on the Exxon Valdez oil spill. *J Geophys Res Oceans* 2010;115:C12077, doi: 10.1029/2010JC006169.
- [26] Li H, Boufadel MC. Long-term persistence of oil from the Exxon Valdez spill in two-layer beaches. *Nature Geosci* 2010;3:96–9.
- [27] Xia Y, Li H, Boufadel MC, Sharifi Y. Hydrodynamic factors affecting the persistence of the Exxon Valdez oil in a shallow bedrock beach. *Water Resour Res* 2010;46:W10528, doi:10.1029/2010WR009179.
- [28] Zhang Q, Volker RE, Lockington DA. Influence of seaward boundary condition on contaminant transport in unconfined coastal aquifers. *J Contam Hydrol* 2001;49:201–15.
- [29] Zhang Q, Volker RE, Lockington DA. Experimental investigation of contaminant transport in coastal groundwater. *Adv Env Res* 2002;6:229–37.

- [30] Boufadel MC, Xia Y, Li H. Modeling solute transport and transient seepage in a laboratory beach under tidal influence. *Env Model Softw* 2011;26:899–912.
- [31] Elfeki AMM, Uffink GJM, Lebreton S. Simulation of solute transport under oscillating groundwater flow in homogeneous aquifers. *J Hydraul Res* 2007;45:254–60.
- [32] Massel SR. Circulation of groundwater due to wave set-up on a permeable beach. *Oceanologia* 2001;43:279–90.
- [33] Jeng D-S, Barry DA, Li L. Water wave-driven seepage in marine sediments. *Adv Water Resour* 2001;24:1–10.
- [34] Voss CI, Provost AM. SUTRA, a model for saturated-unsaturated, variable-density groundwater flow with solute or energy transport. U.S. Geological Survey. Water-Resources Investigations Report, 02-4231, 2002, 250 p., Reston, Virginia, USA. [http://water.usgs.gov/nrp/gwsoftware/sutra\\_2.0/SUTRA\\_2D3D\\_1-documentation.pdf](http://water.usgs.gov/nrp/gwsoftware/sutra_2.0/SUTRA_2D3D_1-documentation.pdf), last accessed 13 November 2012.
- [35] Li L, Barry DA, Pattiaratchi CB, Masselink G. BeachWin: Modeling groundwater effects on swash sediment transport and beach profile changes. *Env Model Softw* 2002;17:313–20.
- [36] Boehm AB, Shellenbarger GG, Paytan A. Groundwater discharge: Potential association with fecal indicator bacteria in the surf zone. *Env Sci Technol* 2004;38:3558–66.
- [37] Bakhtyar R, Ghaheri A, Yeganeh-Bakhtiary A, Barry DA. Process-based model for nearshore hydrodynamics, sediment transport and morphological evolution in the surf and swash zones. *Appl Ocean Res* 2009b;31:44–56.
- [38] Bakhtyar R, Brovelli A, Barry DA, Li L. Wave-induced watertable fluctuations, sediment transport and beach profile change: Modeling and comparison with large-scale laboratory experiments. *Coast Eng* 2011;58:103–18.
- [39] Bakhtyar R, Barry DA, Brovelli A. Numerical experiments on interactions between wave motion and variable-density coastal aquifers. *Coast Eng* 2012;60:95–108.
- [40] Langevin CD, Thorne DT Jr, Dausman AM, Sukop MC, Weixing G. SEAWAT Version 4: A computer program for simulation of multi-species solute and heat transport. U.S. Geological Survey Techniques and Methods Book 6, Chapter A22, 2008, 39 p., <http://pubs.usgs.gov/tm/tm6a22/>, last accessed 13 November 2012.

- [41] Harbaugh AW, Banta ER, Hill MC, McDonald MG. MODFLOW-2000, The US Geological Survey modular groundwater model-User guide to modularization concepts and the groundwater flow process. U.S. Geological Survey, Open File Report 00-92, 2000. <http://water.usgs.gov/nrp/gwsoftware/modflow2000/modflow2000.html>, last accessed 13 November 2012
- [42] Zheng C, Wang PP. MT3DMS: A modular three-dimensional multispecies transport model for simulation of advection, dispersion, and chemical reactions of contaminants in groundwater systems; documentation and user's guide. Contract Rep. SERDP-99-1, U.S. Army Engineering Research Development Center, Vicksburg, Mississippi, 1999, USA, 169 p., <http://hydro.geo.ua.edu/mt3d/index.htm>, last accessed 13 November 2012.
- [43] Bakhtyar R, Barry DA, Yeganeh-Bakhtiary A, Ghaheri A. Numerical simulation of surf-swash zone motions and turbulent flow. *Adv Water Resour* 2009c;32:250-63.
- [44] Bakhtyar R, Barry DA, Yeganeh-Bakhtiary A, Ghaheri A, Li L, Parlange J-Y, Sander GC. Numerical simulation of two-phase flow for sediment transport in the inner-surf and swash zones. *Adv Water Resour* 2010;33:277-90.
- [45] Bakhtyar R, Barry DA, Kees CE. Numerical experiments of breaking waves on contrasting beaches using a two-phase flow method. *Adv Water Resour* 2012;48:68-78.
- [46] Longuet-Higgins MS. Wave set-up, percolation and undertow in the surf zone. *Proc R Soc A* 1983;390:283-91.
- [47] Barry DA, Sposito G. Three-dimensional statistical moment analysis of the Stanford/Waterloo Borden tracer data. *Water Resour Res* 1990;26:1735-45.
- [48] Nielsen P. Tidal dynamics of the watertable in beaches. *Water Resour Res* 1990;26:2127-34.
- [49] Lyard F, Lefevre F, Letellier T, Francis O. Modelling the global ocean tides: Modern insights from FES2004. *Ocean Dyn* 2006;56:394-415.
- [50] Anschutz P, Smith T, Mouret A, Deborde J, Bujan S, Poirier D, Lecroart P. Tidal sands as biogeochemical reactors. *Estuar Coast Shelf Sci* 2009;84:84-90.
- [51] Li L, Barry DA, Pattiaratchi CB. Numerical modelling of tide-induced beach water table fluctuations. *Coastal Eng* 1997;30:105-23.

- [52] Post VEA. A new package for simulating periodic boundary conditions in MODFLOW and SEAWAT. *Comput Geosci* 2011;37:1–7.
- [53] Zheng C, Bennett GD. *Applied Contaminant Transport Modeling*, second ed. Wiley, 2002, New York, USA.
- [54] Diersch H-JG, Kolditz O. Variable-density flow and transport in porous media: Approaches and challenges. *Adv Water Resour* 2002;25:899–944.



## Tables

**Table 1.** Characteristics of the numerical experiments.

Case	Oceanic condition	$H$ (m)	$A$ (m)	$\omega$ (rad d <sup>-1</sup> )	$T$ (s)	$\rho_p$ (g l <sup>-1</sup> )	Solute
1	static sea level	-	-	-	-	998.2	freshwater
2	static sea level	-	-	-	-	1012.5	brackish
3	static sea level	-	-	-	-	1025.0	seawater
4	static sea level	-	-	-	-	1037.5	brine
5	tide	-	0.5	12.57	-	998.2	freshwater
6	tide	-	0.5	12.57	-	1012.5	brackish
7	tide	-	0.5	12.57	-	1025.0	seawater
8	tide	-	0.5	12.57	-	1037.5	brine
9	wave	0.5	-	-	7	998.2	freshwater
10	wave	0.5	-	-	7	1012.5	brackish
11	wave	0.5	-	-	7	1025.0	seawater
12	wave	0.5	-	-	7	1037.5	brine
13	wave + tide	0.5	0.5	12.57	7	998.2	freshwater
14	wave + tide	0.5	0.5	12.57	7	1012.5	brackish
15	wave + tide	0.5	0.5	12.57	7	1025.0	seawater
16	wave + tide	0.5	0.5	12.57	7	1037.5	brine

**Table 2.** Normalized residual solute mass as a function of time and the period of time when 80% of the mass has been removed.

Elapsed time (d)	No oceanic oscillations				Tide				Wave				Combined wave and tide			
	freshwater	brackish	seawater	brine	freshwater	brackish	seawater	brine	freshwater	brackish	seawater	brine	freshwater	brackish	seawater	brine
20	0.523	0.636	0.770	0.828	0.624	0.723	0.799	0.833	0.921	0.993	0.997	1	0.763	0.753	0.833	0.817
40	$2 \times 10^{-4}$	0.001	0.081	0.292	0.003	0.011	0.123	0.314	0.423	0.240	0.396	0.520	0.015	0.016	0.105	0.216
60	$2 \times 10^{-6}$	$8 \times 10^{-5}$	0.008	0.112	$10^{-4}$	0.001	0.018	0.12	0.011	0.008	0.058	0.221	$10^{-4}$	0.001	0.012	0.058
80	$9 \times 10^{-7}$	$3 \times 10^{-5}$	0.002	0.030	$3 \times 10^{-5}$	$4 \times 10^{-4}$	0.005	0.042	$2 \times 10^{-4}$	0.001	0.013	0.098	$3 \times 10^{-5}$	$2 \times 10^{-4}$	0.003	0.016
100	$4 \times 10^{-7}$	$10^{-5}$	0.001	0.009	$10^{-5}$	$10^{-4}$	0.002	0.017	$9 \times 10^{-5}$	$8 \times 10^{-5}$	0.005	0.034	$10^{-5}$	$10^{-4}$	0.001	0.006
120								0.007				0.012				
$t_{80}$ (d) *	24	25	34	48	26	29	45	49	44	42	48	63	29	29	35	41

\*  $t_{80}$  represents the time when 80% of the mass has been removed (residence time).

## Figures

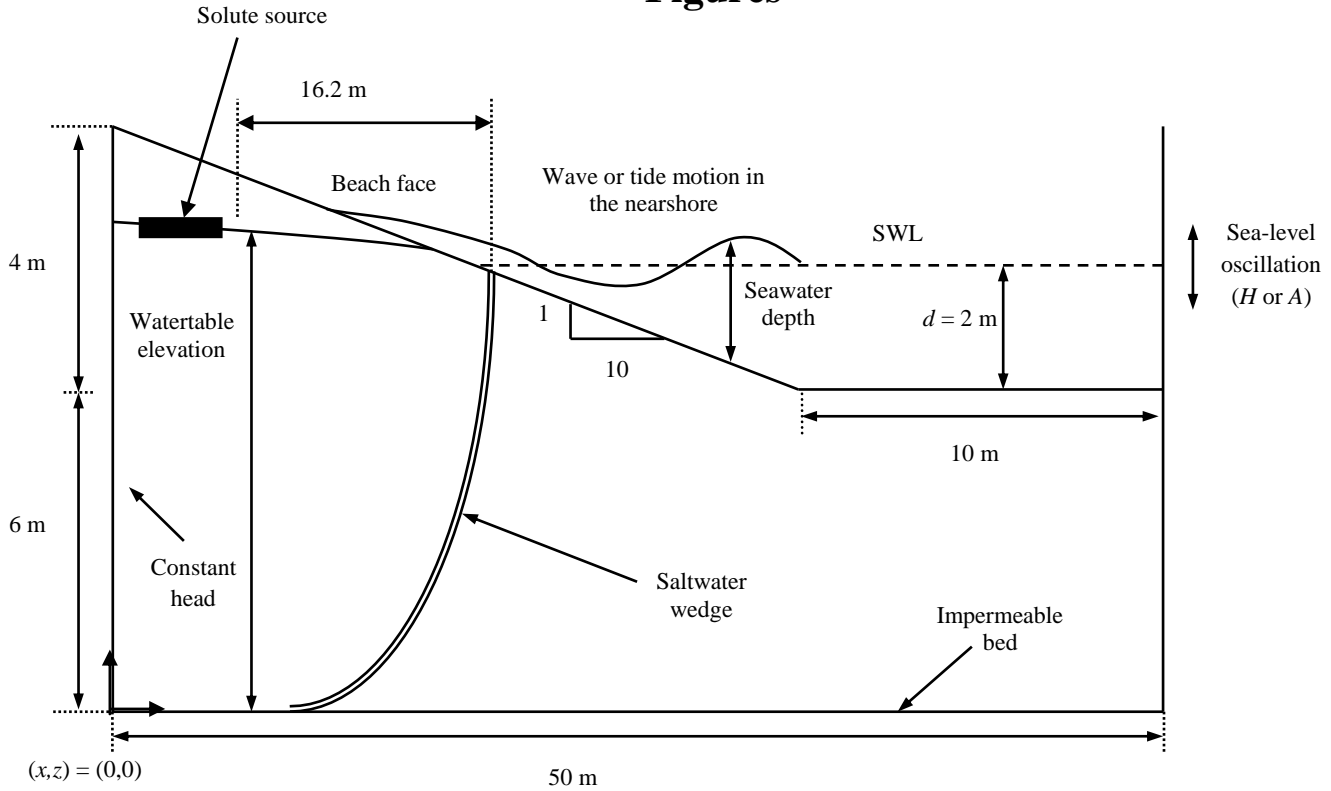


**Figure 1.** Schematic of the numerical model setup (after [39]). The aquifer was unconfined, homogeneous and isotropic with a hydraulic conductivity of  $15 \text{ m d}^{-1}$ . The sand porosity was 0.4 with longitudinal and transversal dispersivity of 0.2 and 0.02 m, respectively [53]. The freshwater and saltwater densities were  $998.2$  and  $1.025 \times 10^3 \text{ kg m}^{-3}$ , respectively. A non-reactive solute was introduced as a line source placed at the watertable at  $2.8 < x < 3.8$  m from the freshwater boundary (16.2-17.3 m from the shoreline). The tracer injection rate was  $0.375 \text{ m}^3 \text{ d}^{-1}$  and lasted 6 d. The double-ended arrow on the right represents the oceanic fluctuations where  $H$  is the wave height and  $A$  is the tidal amplitude. The tidal amplitude was 0.5 m with a semi-diurnal period of 0.5 d. Waves with a height of 0.5 m and a period of 7 s were used to simulate wave forcing (Table 1). A grid spacing of 0.2 m (both directions) was used in all simulations to meet stability constraints (Péclet number  $< 2$ , [54]). The time step was selected automatically to keep the Courant number smaller than 0.75.

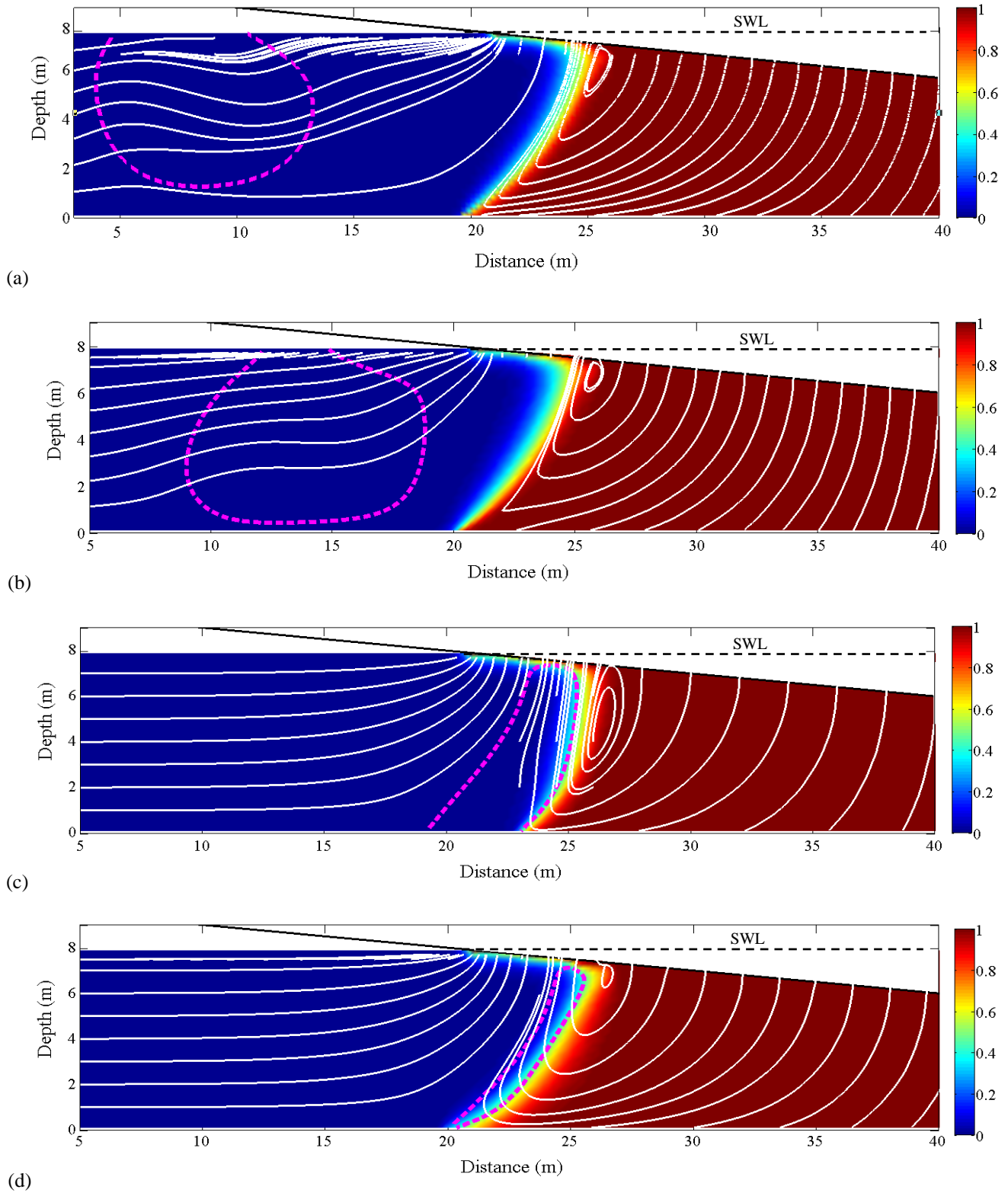


**Figure 2.** Normalized salt concentration, streamlines (in white) and  $0.25C_0$  contour line for the tracer plume (dashed line in magenta) in the aquifer a static sea at different times (5,10,20 and 30 d, respectively). Results are for densest case (Brine, case 4).

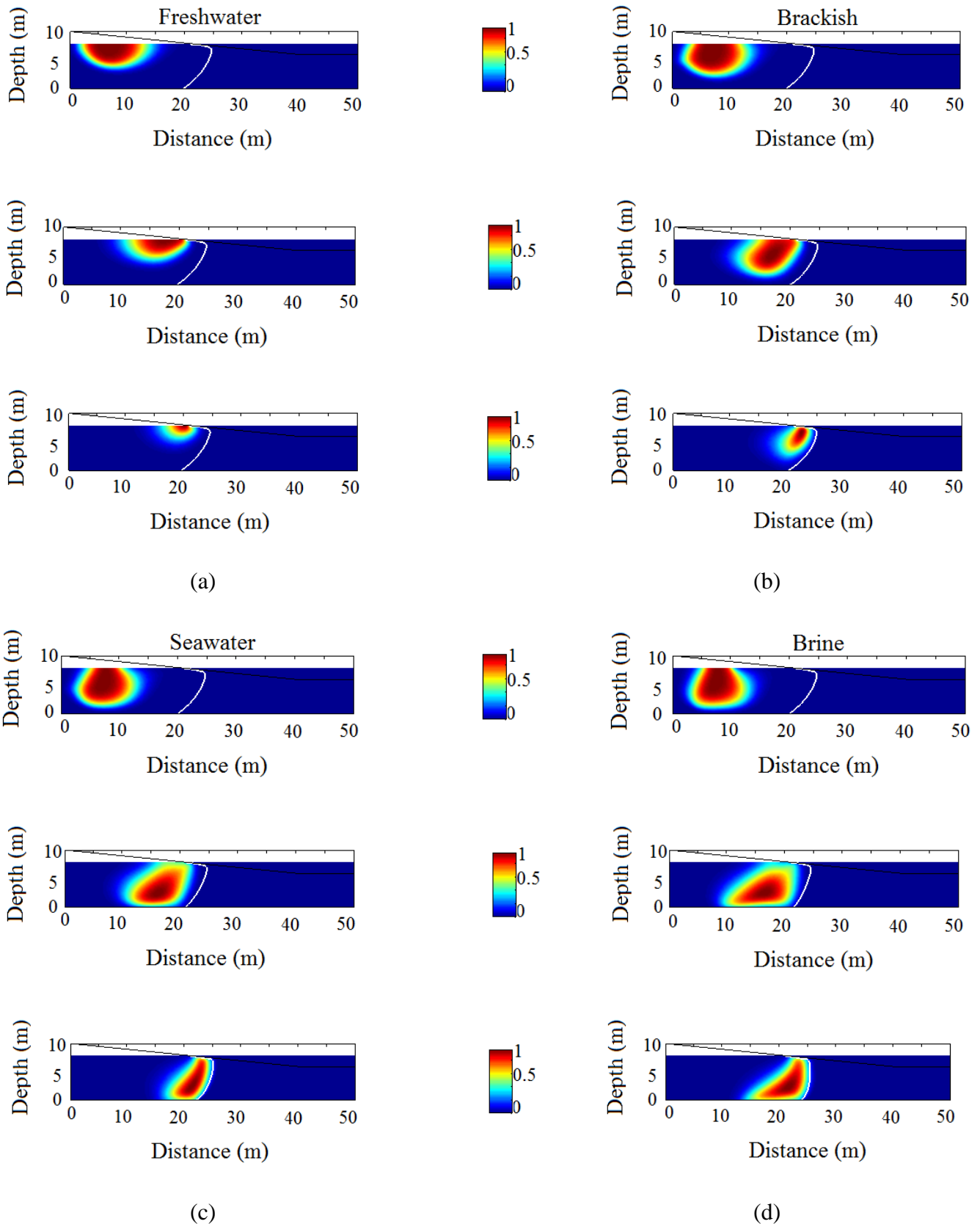
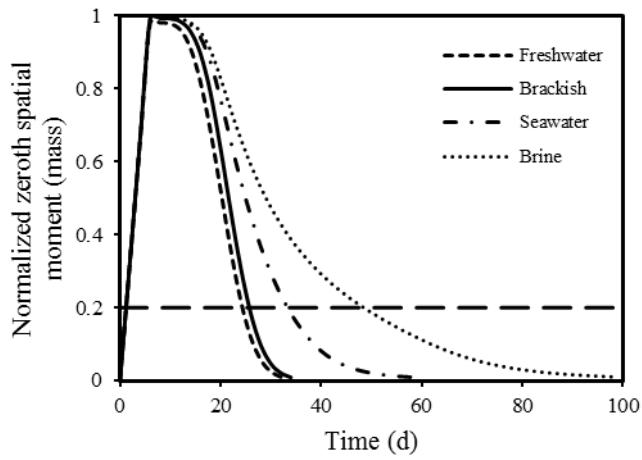
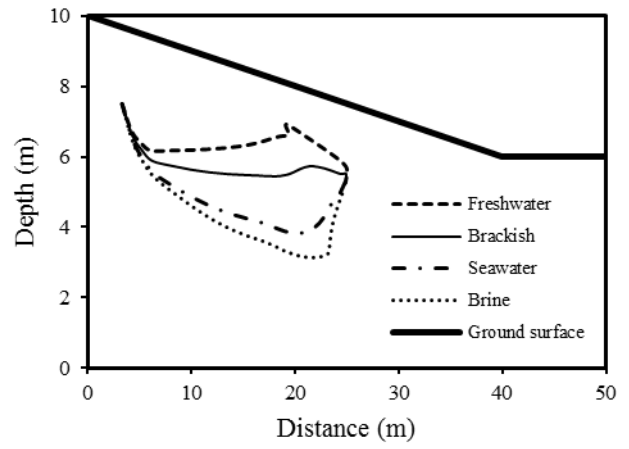


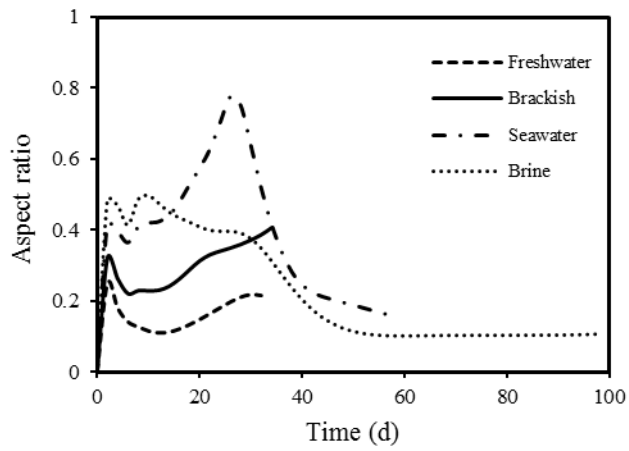
**Figure 3.** Simulated tracer plume in the nearshore aquifer considering solute plume density variations without oceanic forcing: (a) freshwater, case 1; (b) brackish water, case 2; (c) seawater, case 3; and (d) brine, case 4. In all panels, the upper, middle and lower figures show the results after 10, 20 and 30 d, respectively. The color contours represent the relative solute concentration. White lines denote 0.5 normalized seawater concentration contours.



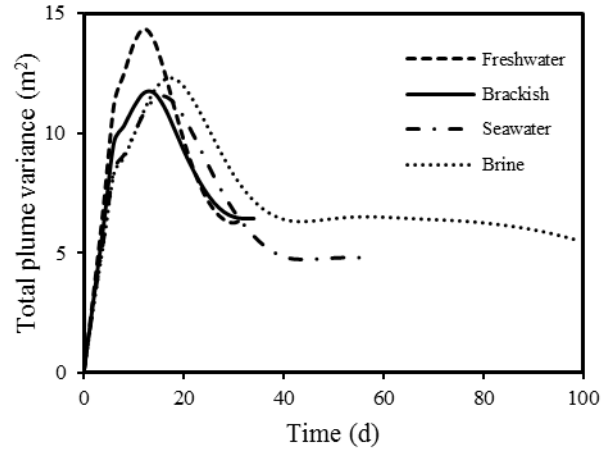
(a)



(b)

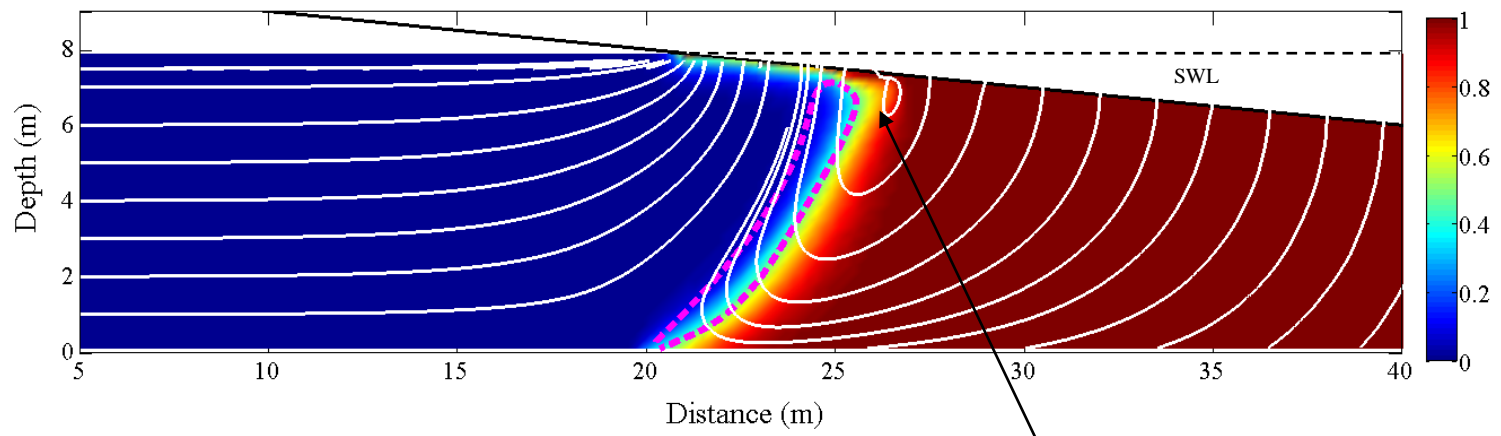


(c)



(d)

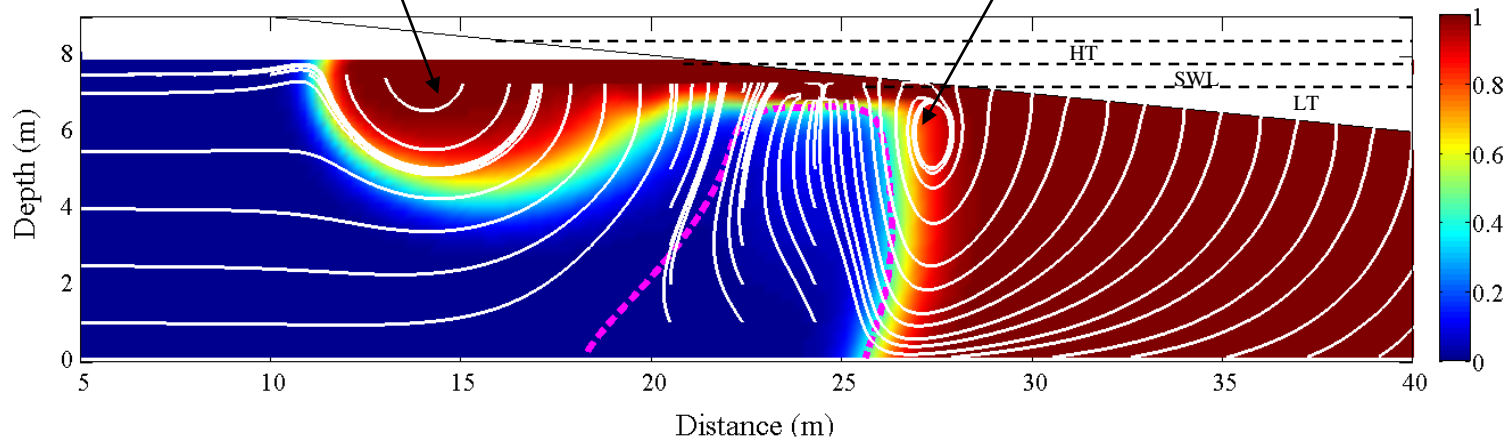
**Figure 4.** Spatial moments of the solute plume in the nearshore aquifer without oceanic forcing and for different densities (cases 1-4, Fig. 3): (a) zeroth moment (total mass), horizontal dashes shows  $t_{80}$ ; (b) evolution of first spatial moment (centroid); (c) aspect ratio; and (d) total plume variance.



Upper saline plume

(a)

Circulation zone below the beach face



(b)

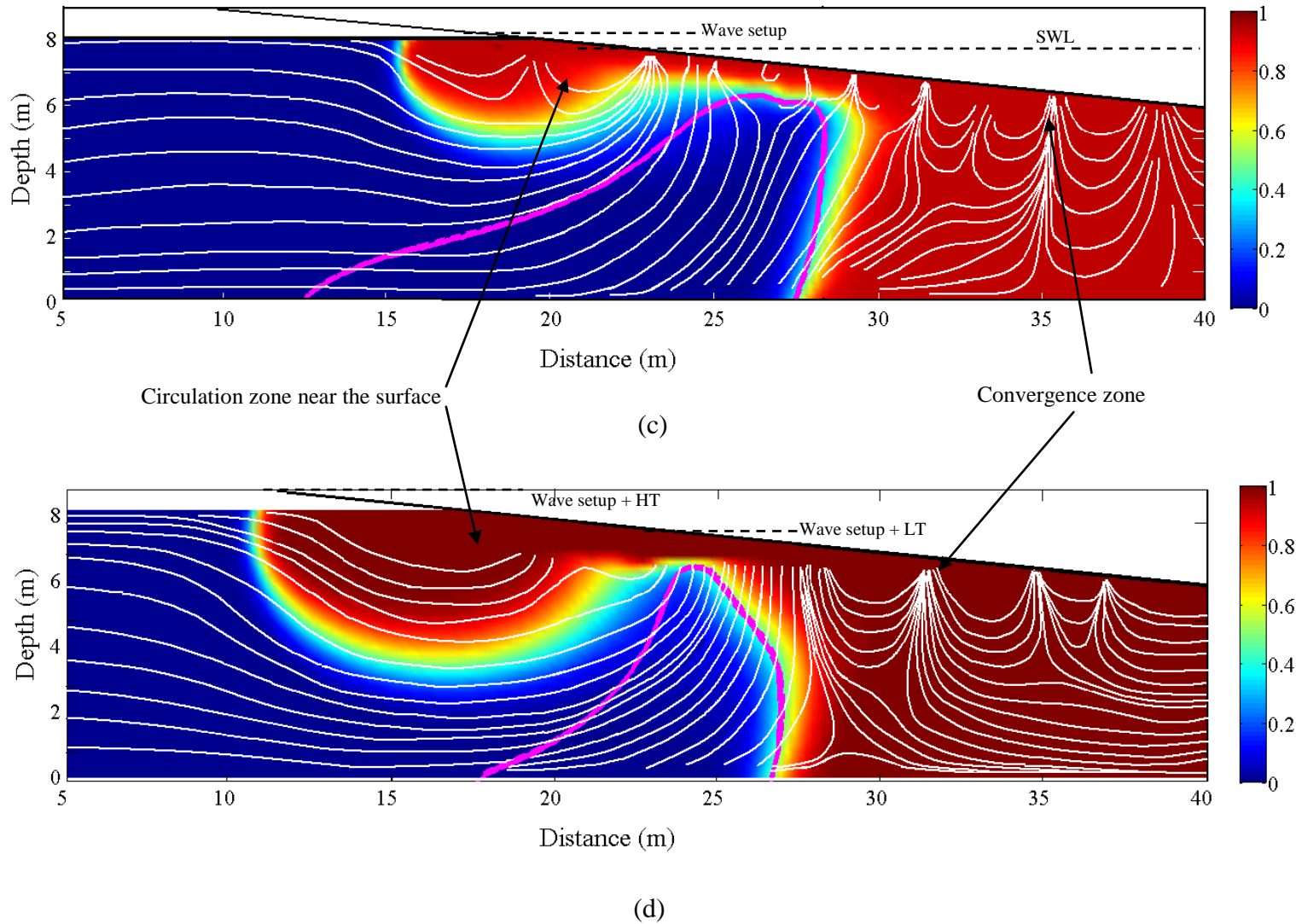


**Figure 5.** Normalized salt concentration, simulated streamlines (in white) and  $0.25C_0$  tracer plume (dashed line, magenta) in the aquifer for different sea-level oscillations: (a) static sea level, case 4; (b) tide, case 8; (c) wave, case 12; (d) combined wave and tide, case 16. All panels show phase-averaged results, after 30 d and for densest case (brine).



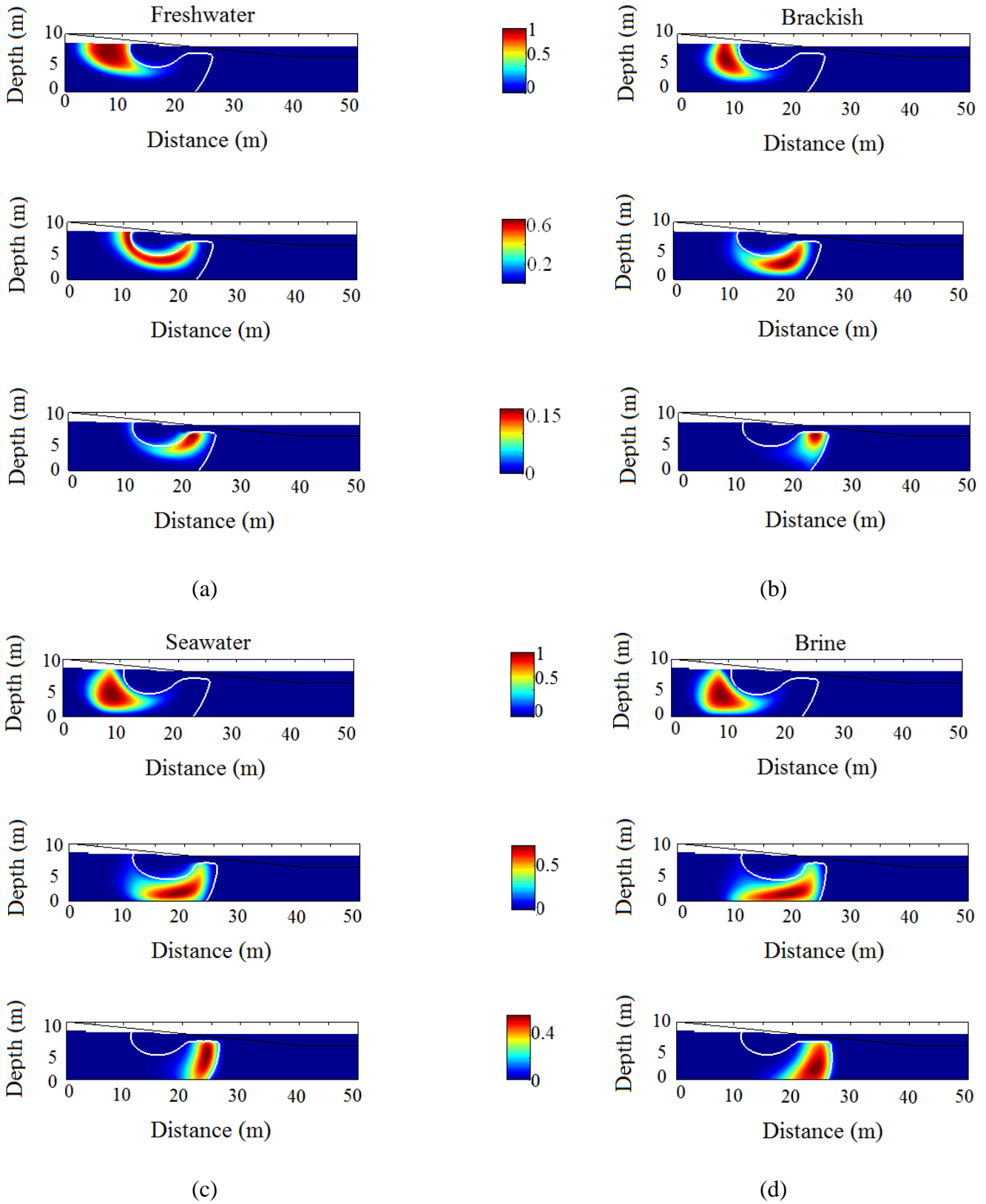
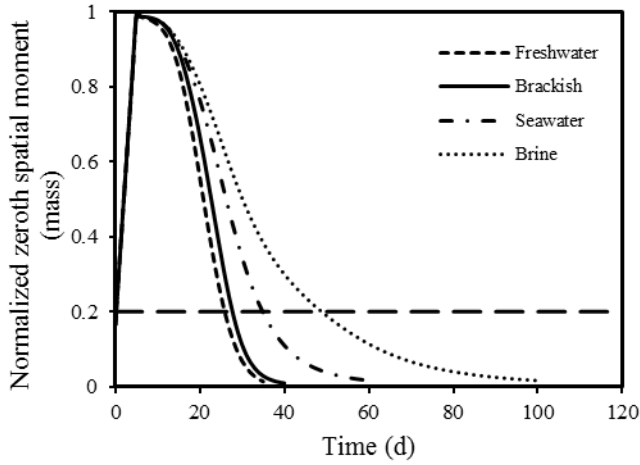
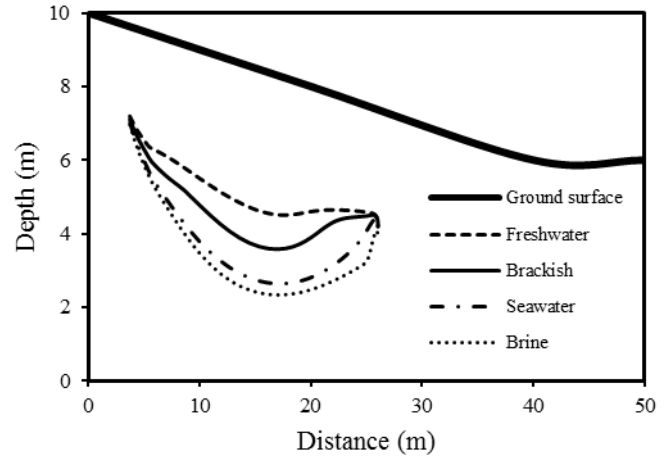


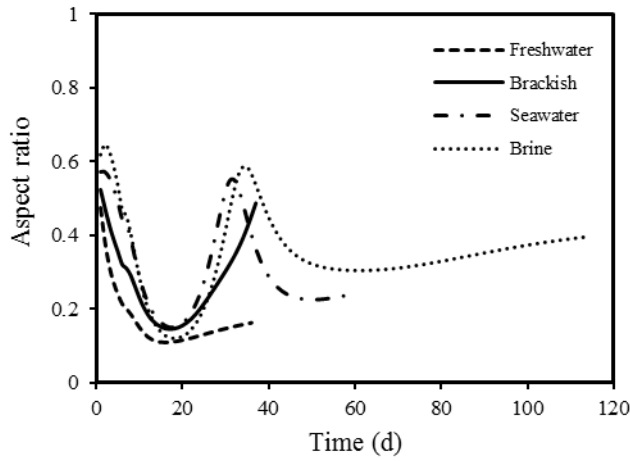
**Figure 6.** Simulated tracer plume in the nearshore aquifer considering solute plume density variations with tidal forcing: (a) freshwater, case 5; (b) brackish water, case 6; (c) seawater, case 7; and (d) brine, case 8. In all panels, the upper, middle and lower figures show the results after 10, 20 and 30 d, respectively. The color contours represent the relative solute concentration. White lines denote 0.5 normalized seawater concentration contours.



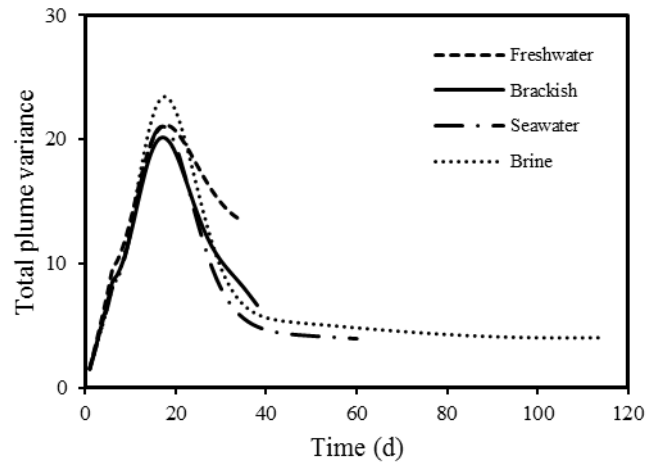
(a)



(b)



(c)



(d)

**Figure 7.** Simulated spatial moments of the solute plume in the nearshore aquifer under tidal forcing and for different densities (cases 5-8, Fig. 6): (a) zeroth moment (total mass), horizontal dash-line shows  $t_{80}$ ; (b) evolution of first spatial moment (centroid); (c) aspect ratio; and (d) total plume variance.

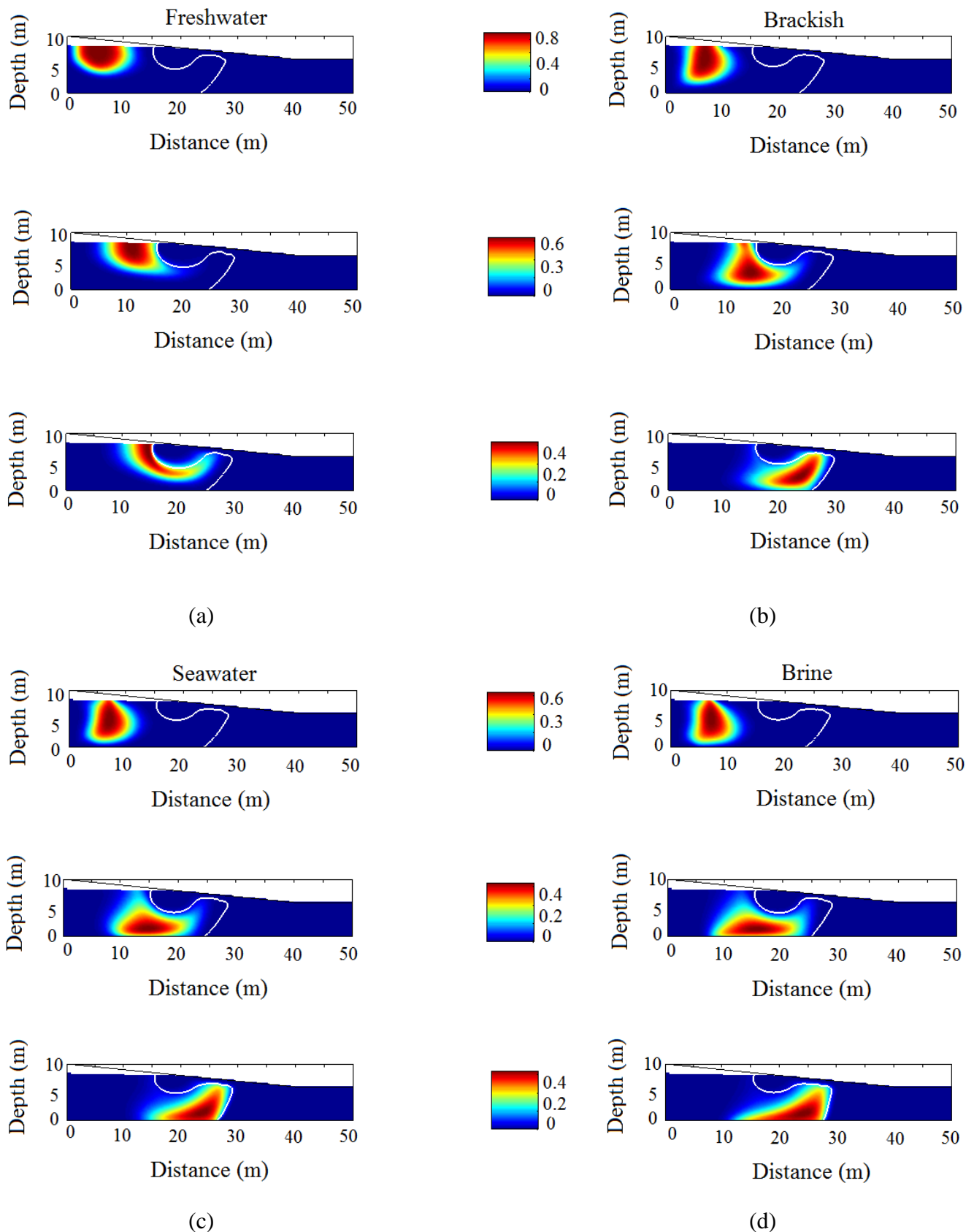


**Figure 8.** Simulated tracer plume in the nearshore aquifer considering solute plume density variations with wave forcing: (a) freshwater, case 9; (b) brackish water, case 10; (c) seawater, case 11; and (d) brine, case 12. In all panels, the upper, middle and lower figures show the results after 10, 20 and 30 d, respectively. The color contours represent the relative solute concentration. White lines denote 0.5 normalized seawater concentration contours.

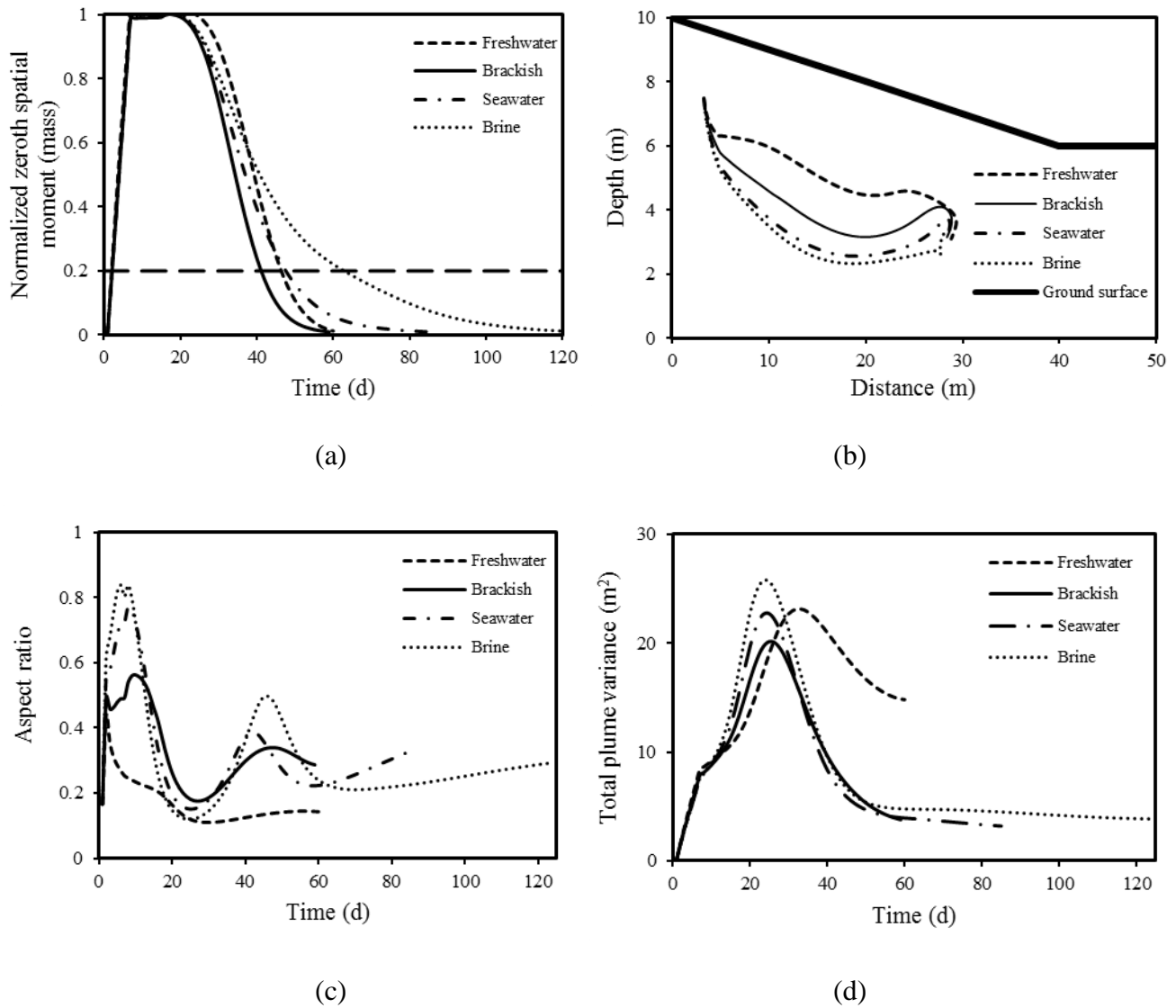


**Figure 9.** Simulated spatial moments of the solute plume in the nearshore aquifer under waves (cases 9-12, Fig. 8): (a) zeroth moment (total mass), horizontal dash-line shows  $t_{80}$ ; (b) evolution of first spatial moment (centroid); (c) aspect ratio; and (d) total plume variance.

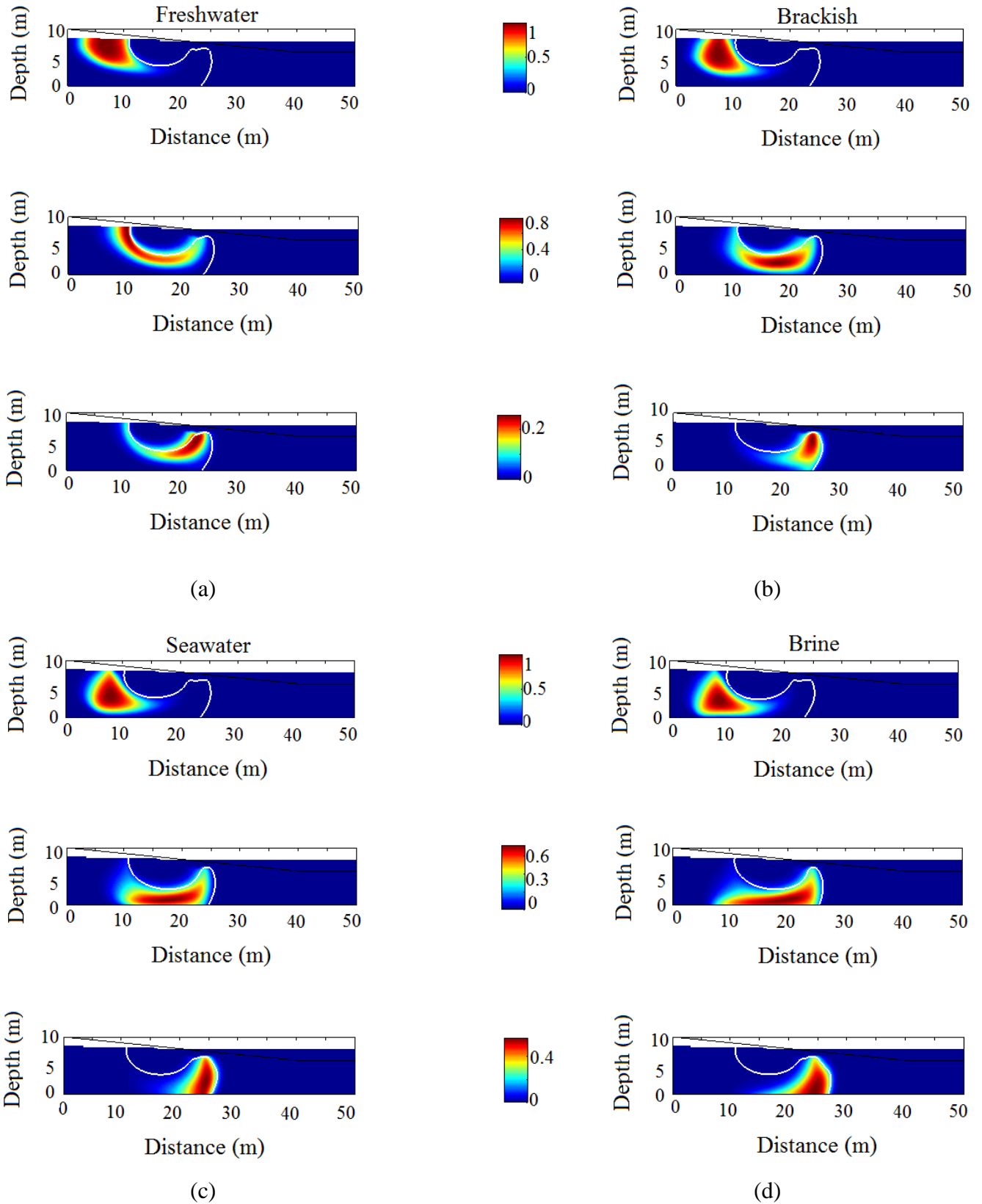
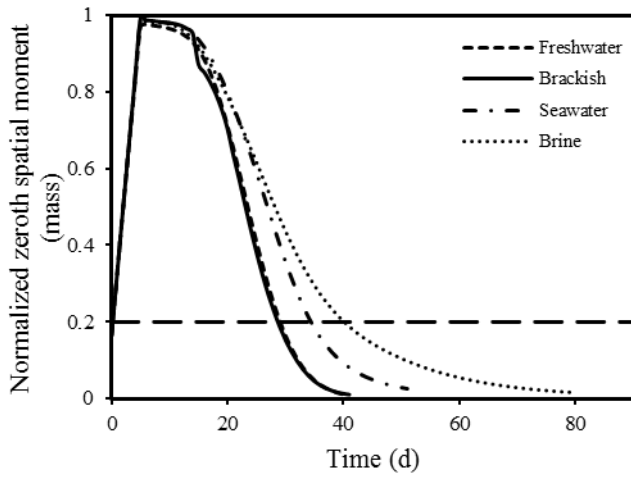
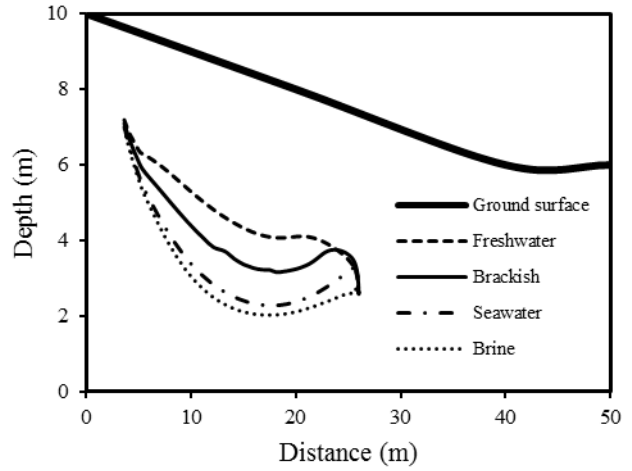


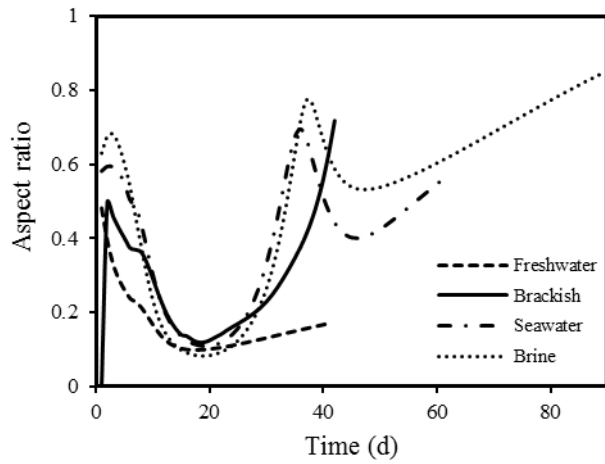
**Figure 10.** Simulated tracer plume in the nearshore aquifer considering solute plume density variations under combined wave and tide: (a) freshwater, case 13; (b) brackish water, case 14; (c) seawater, case 15; and (d) brine, case 16. In all panels, the upper, middle and lower figures show the results after 10, 20 and 30 d, respectively. The color contours represent the relative solute concentration. White lines denote 0.5 normalized seawater concentration contours.



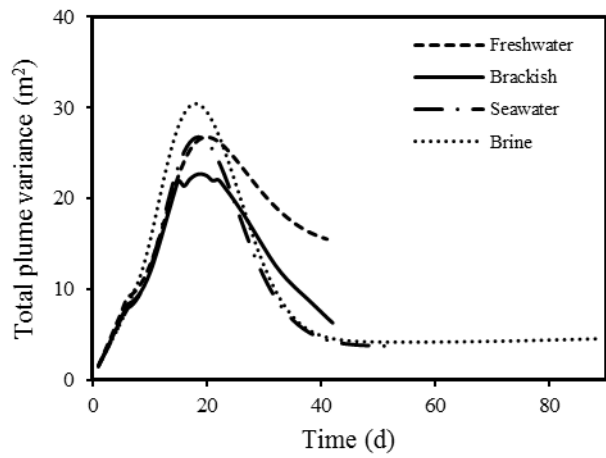
(a)



(b)

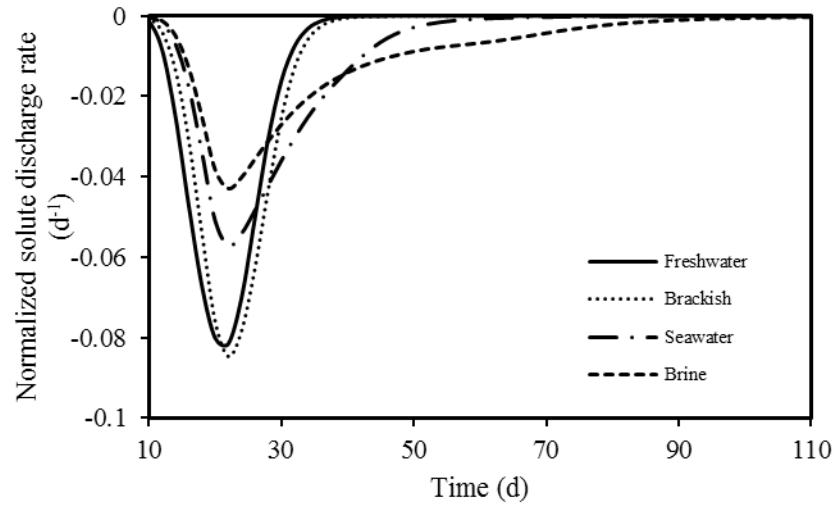


(c)

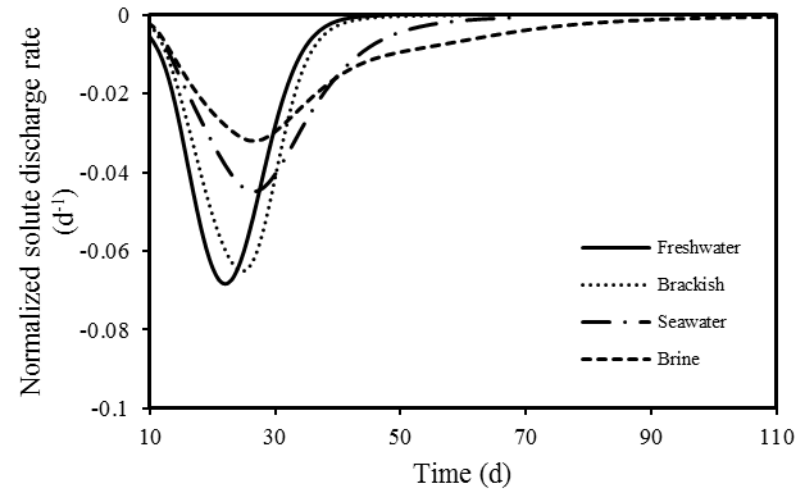


(d)

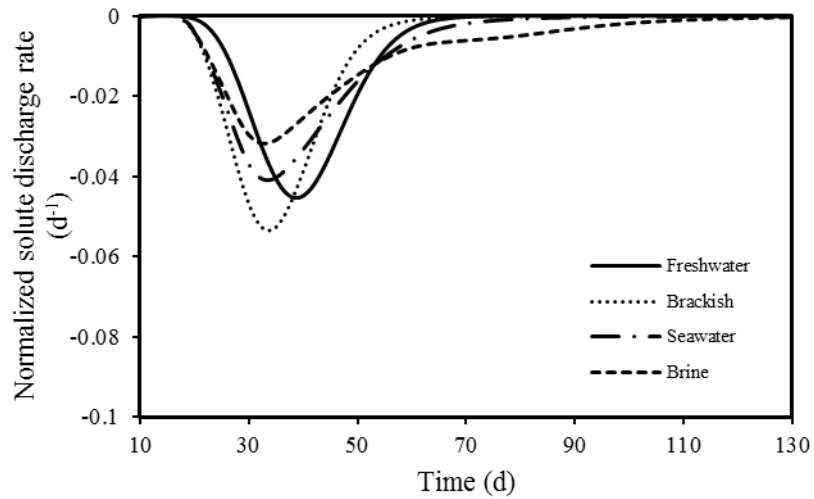
**Figure 11.** Simulated spatial moments of the solute plume in the nearshore aquifer under combined wave and tide forcing (cases 13-16, Fig. 10): (a) zeroth moment (total mass), horizontal dash-line shows  $t_{80}$ ; (b) evolution of first spatial moment (centroid); (c) aspect ratio; and (d) total plume variance.



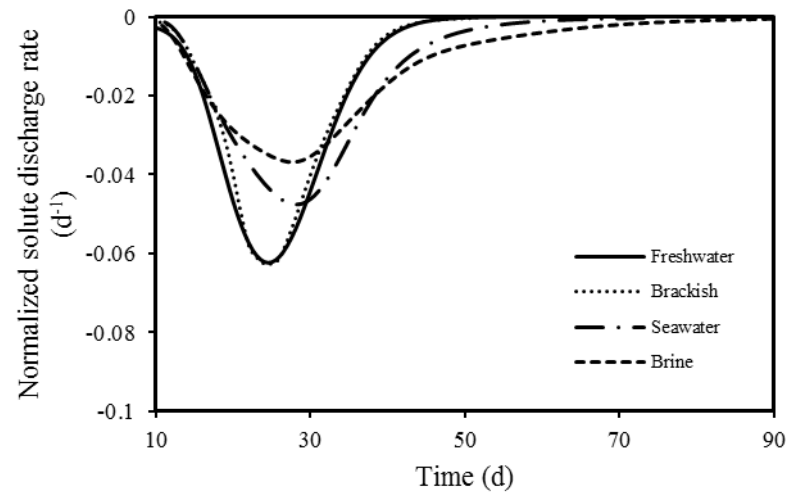
(a)



(b)



(c)



(d)

**Figure 12.** Solute discharge rate across the beach face: (a) no oceanic forcing; (b) tide; (c) wave; and (d) combined wave and tide, where vertical axis is the rate of change of the mass (normalized by the initial mass) of solute in the aquifer over time).